Acta Crystallographica Section A
Foundations of Crystallography
ISSN 0108-7673

Received 12 July 2008
Accepted 19 July 2009

Multiresolution of quasicrystal diffraction spectra

Avi Elkharrat,[a] Jean-Pierre Gazeau[a]* and Françoise Dénoyer[b]

[a]Boite 7020, APC, CNRS UMR 7164, Université Paris Diderot Paris 7, 75205 Paris Cedex 13, France, and [b]LPS, CNRS UMR 8502, Université Paris-Sud, France. Correspondence e-mail: gazeau@apc.univ-paris7.fr

A method for analyzing and classifying two-dimensional pure point diffraction spectra (*i.e.* a set of Bragg peaks) of certain self-similar structures with scaling factor $\beta > 1$, such as quasicrystals, is presented. The two-dimensional pure point diffraction spectrum Π is viewed as a point set in the complex plane in which each point is assigned a positive number, its Bragg intensity. Then, by using a nested sequence of self-similar subsets called β-lattices, we implement a multiresolution analysis of the spectrum Π. This analysis yields a partition of Π simultaneously in geometry, in scale and in intensity (the 'fingerprint' of the spectrum, not of the diffracting structure itself). The method is tested through numerical explorations of pure point diffraction spectra of various mathematical structures and also with the diffraction pattern of a realistic model of a quasicrystal.

1. Introduction

The absence of periodicity in quasicrystalline structures demands new mathematical tools. From the very first experimental evidence of quasicrystals (Shechtman *et al.*, 1984) it became necessary to build a pertinent theory of aperiodic point sets and tilings and a spectral analysis for diffraction or for electronic transport suited to the self-similarity shown by quasicrystals (Janot, 1996; Baake & Moody, 2000). In fact, an appealing mathematical program, combining number theory, free groups and semi-groups, measure theory and harmonic analysis, has been developing strongly for the past 25 years.

One of these mathematical approaches is based on the concepts of β-integer and β-lattice, where $\beta > 1$ can be equal to one of the following quadratic algebraic numbers: $\tau = (1 + 5^{1/2})/2$ (for five and tenfold symmetry), $\delta = 1 + 2^{1/2} = 1 + 2\cos(2\pi/8)$ (for octagonal symmetry) and $\theta = 2 + 3^{1/2} = 2 + 2\cos(2\pi/12)$ (for dodecagonal symmetry). Each such β determines a discrete set of the line, $\mathbb{Z}_\beta$, the set of β-integers (Burdík *et al.*, 1998), which play the role of integers in the study of quasicrystalline structures. β-Lattices are based on β-integers in the same way as lattices are based on integers:

$$\Gamma = \sum_{i=1}^{d} \mathbb{Z}_\beta \mathbf{e}_i,$$

with $(\mathbf{e}_i)$ a base of $\mathbb{R}^d$. In specific situations, decorated versions $\widetilde{\mathbb{Z}}_\beta = \mathbb{Z}_\beta$ + finite set F will be used instead. These (decorated) β-lattices are eligible frames in which one could think of the properties of quasiperiodic point sets and tilings, thus generalizing the notion of lattice in periodic cases.

In this paper we present a new method for analyzing the pure point parts (Bragg peaks) of diffraction patterns for aperiodic point sets supported by β-lattices. The method rests upon the counting framework provided by β-integers and β-lattices and their self-similarity property,

$$\beta\mathbb{Z}_\beta \subset \mathbb{Z}_\beta, \ \rightarrow \ \beta\Gamma \subset \Gamma.$$

This property allows one to consider the infinite nested sequence

$$\ldots \subset \Gamma/\beta^{j-1} \subset \Gamma/\beta^{j} \subset \Gamma/\beta^{j+1} \subset \ldots, \qquad (1)$$

as a multiresolution filter for the point set we have to examine. The term multiresolution is borrowed from discrete wavelet analysis (Mallat, 1989), in which analogous sequences of scaled discretizations of the real line and related sequences of Hilbert spaces yield an efficient filter for analyzing signals. Multiresolution sequences [equation (1)] allow one to build 'catalogues' of diffraction patterns for standard or manageable well identified site-occupation distributions. We would like to introduce the idea of a sort of identity card for the diffraction pattern of a quasiperiodic set. Having at our disposal such catalogues of 'diffraction fingerprints', one can then examine experimental diffraction patterns – those displayed by real quasicrystals or other more or less exotic structures. The next step should be a (patient!) labor of comparison, classification and identification. However, we do not investigate the (difficult) question of complete determination of the real structure, related to some extent to the homometry problem, and we do not examine the Patterson function either.

This article is organized as follows. In §2 we give the necessary preliminaries to this work, namely the mathematical expressions defining diffraction patterns of point sets, and the definitions of algebraic cyclotomic rings, which are dense point sets supporting Bragg peaks of the structures considered. Appendix *A* presents relevant mathematical definitions and properties, particularly those concerning the aforementioned

three scaling factors appearing in observed quasicrystals. In §3 we introduce the β-lattices whose construction is based on the numeration system associated with the number $\beta > 1$ and its corresponding set of β-integers. Mathematical explanations are found in Appendices *B* and *C*. We then show how to describe the above cyclotomic rings as limits of nested sequences of inflated/deflated versions of β-lattices. This notion of limit should here be accepted in the following sense.

Definition 1. Let Δ be a dense set and $(\Delta_j)_{j\in\mathbb{Z}}$ a nested sequence of Delone (Delaunay) sets such that

$$\ldots \subset \Delta_{j-1} \subset \Delta_j \subset \Delta_{j+1} \subset \ldots \subset \Delta.$$

One says that Δ is the (inductive) limit of the sequence $(\Delta_j)_{j\in\mathbb{Z}}$ if, for all $x \in \Delta$, there exists a $j \in \mathbb{Z}$ such that $x \in \Delta_j$, *i.e.* if Δ is equal to the countable union of the (Δ_j)'s:

$$\Delta = \bigcup_{j\in\mathbb{Z}} \Delta_j.$$

The cut-and-project sets, *i.e.* projections of strips (with irrational directions) of higher-dimensional lattices, have become standard models for quasicrystals. We show in §4 to what extent they can be considered as subsets of our β-lattices, and this naturally leads to the notion of weighted Dirac measures supported by β-lattices. We present in §5 the general framework of our multiresolution analysis of Bragg-peak sets through nested sequences of β-lattices, and the precise description of its implementation is given in §6, more precisely in relation with the indexation of Bragg peaks. The detailed results of our numerical investigations are presented in §7. We first analyze academic models, such as the diffraction patterns of β-lattices themselves or of simple cut-and-project sets embedded in these β-lattices, like those with pentagonal or decagonal symmetries. We also examine more elaborate cut-and-project sets like the set of vertices of Penrose tilings. We then turn our attention to a point set closer to realistic models for an experimental AlCuCo quasicrystal, namely the Steurer and Kuo model. In conclusion, we discuss the presented results, emphasizing what we consider as promising directions or developments in the future.

Concerning the mathematical material needed for understanding our approach, we have attempted to minimize the amount of technical details within the main body of the paper. The aim of the appendices is to provide readers unfamiliar with these objects with enough definitions and properties to understand our approach.

2. Diffraction spectra and cyclotomic rings

Let Λ be a discrete set of points in $\mathbb{R}^d$, and suppose that the diffraction spectrum of Λ admits a pure point part. In reciprocal space, the function giving the intensity per diffracting site is the limit

$$I(k) \equiv I_k = \lim_{L\to\infty} \left|c_k^L\right|^2, \qquad (2)$$

where Λ_L is the restriction of Λ on a d-dimensional ball of radius L (or equivalently a d-dimensional cube of side L) centered at the origin, and $c_k^L = [1/\mathrm{Card}(\Lambda_L)] \sum_{\lambda\in\Lambda_L} \exp(-ik\lambda)$ is the Fourier coefficient of Λ in an average sense for the wavevector k. It has been known since Hof (1995) and Schlottmann (1998, 2000) that if Λ is a cut-and-project set, its diffraction measure, *i.e.* the Fourier transform of its unique autocorrelation measure, is pure point, and is well described by the above formula, which reads as the distribution

$$I = \sum_{k\in\Lambda^*} I_k \delta_k,$$

where δ_k is the Dirac delta function at k. The set $\Lambda^* \subset \mathbb{R}^d$ is the support of all Bragg peaks in the diffraction spectrum, and is generically dense in reciprocal space. We can say with some abuse of terminology that Λ^* is the reciprocal lattice of Λ. A Bragg peak is then defined by the weighted Dirac measure $I_k\delta_k$. In this article we will rather employ the following notation, combining intensity with geometry, for designating a Bragg peak:

$$p = (k, I_k).$$

Denote by $\mathcal{I}$ the range of intensities of Bragg peaks. Of course, $\mathcal{I}$ is bounded. Then the Bragg spectrum, or pure point spectrum, of a diffractive structure is the graph of the map $k \mapsto I_k$, *i.e.*

$$\Pi = \{p = (k, I_k) \mid k \in \Lambda^*,\ I_k \in \mathcal{I}\} \subset \Lambda^* \times \mathcal{I}. \qquad (3)$$

(It might happen in the following that index k is dropped for conciseness). There exists a maximal intensity, $I_{\max} = \max(\mathcal{I})$. This maximum is determined by experimental data and provides the whole spectrum with a natural unit. All points supporting $I_{\max}$ are symmetry centers for Λ^* with (at least) respect to space inversion.

Example 1. Suppose Λ is a point set representing some cubic monoatomic crystal, then $\Lambda^* = \mathbb{Z}^3$ and $\mathcal{I} = \{I_0 = I_{\max}\}$. Hence $\Pi = \{p = ((n_1, n_2, n_3), I_0) \mid n_i \in \mathbb{Z}\}$ is the diffraction spectrum of such a structure. More elaborate periodic pure point diffraction spectra are obtained from decorated lattices of this type.

Example 2. A less trivial example is provided by the diffraction spectrum of the set of vertices of a Penrose tiling. The support of the diffraction spectrum (in suitable units) is then the dense point set of the cyclotomic integers $\mathbb{Z}[\exp[i(\pi/5)]] = \sum_{q=0}^{4} \mathbb{Z}\exp[iq(\pi/5)]$ (see Appendix *A*), the range of intensities is the set $\mathcal{I} = (0, I_{\max}]$, and there exists one and only one point supporting $I_{\max}$.

In the following we will restrict ourselves to the study of two-dimensional structures, and will then adopt complex notations. In certain situations for which a point set $\Lambda \subset \mathbb{C}$ admits some (at least local) rotational symmetry of order N, the reciprocal lattice of Λ is given by $\Lambda^* = \alpha\mathbb{Z}[\zeta]$, where α is some scaling factor we shall discard in the following, and where $\mathbb{Z}[\zeta]$ is the cyclotomic extension ring of the Nth root of unity $\zeta = \exp(i2\pi/N)$ given by

$$\mathbb{Z}[\zeta] = \sum_{q=0}^{N-1} \mathbb{Z}\zeta^q = \mathbb{Z}[2\cos(2\pi/N)] + \mathbb{Z}[2\cos(2\pi/N)]\zeta.$$

The set

$$\mathbb{Z}[\rho \equiv 2\cos(2\pi/N)] \stackrel{\text{def}}{=} \{m_1 + m_2\rho + \ldots + m_{q_N}\rho^{q_N-1} \mid m_1, m_2, \ldots, m_{q_N} \in \mathbb{Z}\}$$

is defined as the extension ring on the integers of the algebraic integer $2\cos(2\pi/N)$, with q_N the degree of its minimal polynomial.

The set $\mathbb{Z}[\zeta]$ is generically dense in $\mathbb{C}$, except for crystallographic cases: $2\cos(2\pi/N) \in \mathbb{N}$ if and only if $N = 1, 2, 3, 4$ or 6. If this condition is satisfied then $\mathbb{Z}[\zeta]$ is a discrete periodic subset of the complex plane. More details on definitions and properties are given in Appendix *A*.

In the noncrystallographic cases, we will focus on a class of numbers called cyclotomic Pisot–Vijayaraghavan (PV) numbers, as they appear naturally in quasicrystallographic systems (Barache *et al.*, 1998). PV numbers are defined in Appendix *A*. We need to discriminate between the two cases in which the constant term in their minimal polynomial is -1 or 1. The notations in the following list of quasicrystallographic PV numbers (together with their minimal polynomial) will be kept throughout the rest of the article.

Notation 1. If β is a quadratic Pisot number, then we denote by β' its Galois conjugate, *i.e.* the other root of the minimal polynomial associated with β.

Case 1:

$$N = 5, 10: \quad \tau = (1 + 5^{1/2})/2 = 1 + 2\cos(2\pi/5) = 2\cos(2\pi/10), \quad \tau' = -1/\tau, \quad X^2 - X - 1. \tag{4}$$

$$N = 8: \quad \delta = 1 + 2^{1/2} = 1 + 2\cos(\pi/4), \quad \delta' = -1/\delta, \quad X^2 - 2X - 1. \tag{5}$$

Case 2:

$$N = 5, 10: \quad \gamma = \tau^2 = (3 + 5^{1/2})/2 = 2 + 2\cos(2\pi/5) = 1 + 2\cos(2\pi/10), \quad \gamma' = 1/\gamma, \quad X^2 - 3X + 1. \tag{6}$$

$$N = 12: \quad \theta = 2 + 3^{1/2} = 2 + 2\cos(\pi/6), \quad \theta' = 1/\theta, \quad X^2 - 4X + 1. \tag{7}$$

Note that in the case $N = 7$, we have $\beta = 1 + 2\cos(2\pi/7)$, which is a solution to the cubic equation $X^3 - 2X^2 - X + 1 = 0$, but which has not yet been really encountered in stable structures.

3. β-Lattice sequences converging to cyclotomic rings

Let Λ be an aperiodic crystal for which the inflation properties are governed by an algebraic number β. The β-lattices constitute an underlying structure, allowing one to somehow partially recover the description one would have if Λ were a periodic crystal (Burdík *et al.*, 1998; Elkharrat *et al.*, 2004). In this section we introduce the notion of a β-lattice, together with the partition of cyclotomic rings it generates.

3.1. β-Lattices

Roughly speaking, given $\beta > 1$, β-integers are all numbers that are polynomial when written in base β. They form the countable point set $\mathbb{Z}_\beta \subset \mathbb{R}$. They are to β-lattices what integers $\mathbb{Z}$ are to lattices. Mathematical definitions and properties are given in Appendix *B*. When *N* is quasicrystallographic, *i.e.* N = 5, 10, 8 or 12, respectively associated with one of the numbers $\beta = \tau$, δ and θ, the corresponding sets $\mathbb{Z}_\beta$ enjoy remarkable properties (Burdík *et al.*, 1998). We then adopt the generic name β-lattice for higher-dimensional point sets of the form

$$\Gamma_\beta = \sum_{i=1}^{d} \mathbb{Z}_\beta \mathbf{e}_i$$

with $(\mathbf{e}_i)_{1\le i\le d}$ a basis of $\mathbb{R}^d$. By construction, this set is self-similar and symmetrical with respect to the origin:

$$\beta\Gamma_\beta \subset \Gamma_\beta, \quad \Gamma_\beta = -\Gamma_\beta. \tag{8}$$

We now focus on the following two-dimensional β-lattices.

Case 1:

$$\Gamma_\beta = \mathbb{Z}_\beta + \mathbb{Z}_\beta\zeta$$

with $\zeta = \exp[i(2\pi/10)]$ for $\beta = \tau$ and $\zeta = \exp[i(2\pi/8)]$ for $\beta = \delta$.

Case 2:

One needs to work with decorated β-lattices involving the decorated β-integers $\widetilde{\mathbb{Z}}_\beta = \mathbb{Z}_\beta + \{0, \pm 1/\beta\}$. The latter are described in Appendix *C*.

$$\widetilde{\Gamma}_\beta = \widetilde{\mathbb{Z}}_\beta + \widetilde{\mathbb{Z}}_\beta\zeta$$

with $\zeta = \exp[i(2\pi/10)]$ or $\zeta = \exp[i(2\pi/5)]$ for $\beta = \gamma$, and $\zeta = \exp[i(2\pi/12)]$ for $\beta = \theta$.

It should be noticed at this point that these β-lattices are endowed with rich arithmetic and algebraic properties [details are given in Elkharrat *et al.* (2004) and references therein]. Although the sets Γ_β are not rotationally invariant, they contain after suitable rescaling or decoration rotationally invariant sets like cut-and-project sets (see §4) with a rotationally invariant window, or sets like $\cup_{q=0}^{N-1}\Gamma_\beta\zeta^q$ and $\sum_{q=0}^{N-1}\mathbb{Z}_\beta\zeta^q$ with N = 8, 10 or 12, respectively. This results from the following inclusions for $q = 1, 2, \ldots, N-1$:

$$\zeta^q\Gamma_\tau \subset \frac{\Gamma_\tau}{\tau^2}, \quad \zeta^q\Gamma_\delta \subset \frac{\Gamma_\delta}{\delta^3}, \quad \zeta^q\Gamma_\theta \subset \widetilde{\widetilde{\Gamma}}(\theta) \equiv \widetilde{\widetilde{\mathbb{Z}}}_\theta + \widetilde{\widetilde{\mathbb{Z}}}_\theta\zeta, \tag{9}$$

where $\widetilde{\widetilde{\mathbb{Z}}}_\theta = \mathbb{Z}_\theta + \{0, \pm 1/\theta, \pm 2/\theta\}$.

In order to give explicit results for the limit of nested sequences of scaled/decorated versions of β-lattices, we need to deal with the image of β-lattices through Galois conjugation, *i.e.* the image of β-lattices in internal space. Hence, it is possible to extend Galois conjugation and related properties given in Appendix *C* [see equation (34) and following equations] to two-dimensional structures (Moody & Patera, 1994),

$$z = m + n\beta + (p + q\beta)\zeta \mapsto z' = m + n\beta' + (p + q\beta')\zeta^r,$$

where $r = 3$ for $\beta = \tau$, δ and γ, and $r = 5$ for $\beta = \theta$. Let R_β denote the rhomboid convex hulls given by

$$R_\beta = [-1, 1] + [-1, 1]\zeta \quad \text{(case 1)},$$

$$R_\beta = [-\beta, \beta] + [-\beta, \beta]\zeta \quad \text{(case 2)}.$$

Then we derive from equations (35) and (36) the following characterizations of internal spaces:

$$\mathbb{Z}[\zeta] \cap R_\beta = (\Gamma_\beta)' \cap R_\beta \quad \text{(case 1)}, \tag{10}$$

$$\mathbb{Z}[\zeta] \cap R_\beta = (\widetilde{\Gamma}_\beta)' \cap R_\beta \quad \text{(case 2)}. \tag{11}$$

More prosaically, any element of the dense cyclotomic ring $\mathbb{Z}[\zeta]$ lying within the domain R_β is the conjugate of an element of the discrete set Γ_β (respectively $\widetilde{\Gamma}_\beta$). In Figs. 1, 2 and 3 we display the τ-lattice Γ_τ, the δ-lattice Γ_δ and the decorated θ-lattice, $\widetilde{\Gamma}_\theta$, respectively, all three as point sets and as tilings. We also show their respective internal spaces.

3.2. Nested sequences of β-lattices

In Appendix *C* we prove the following decompositions of the extension rings $\mathbb{Z}[\beta]$ for quasicrystalline β.

Case 1:

$$\lim_{j\to\infty}\left(\mathbb{Z}_\beta/\beta^j\right) = \bigcup_{j\in\mathbb{Z}}\left(\mathbb{Z}_\beta/\beta^j\right) = \mathbb{Z}[\beta]. \tag{12}$$

Case 2:

$$\lim_{j\to\infty}\left(\widetilde{\mathbb{Z}}_\beta/\beta^j\right) = \bigcup_{j\in\mathbb{Z}}\left(\widetilde{\mathbb{Z}}_\beta/\beta^j\right) = \mathbb{Z}[\beta], \tag{13}$$

where $\widetilde{\mathbb{Z}}_\beta = \mathbb{Z}_\beta + \{0, \pm 1/\beta\}$.

Note that in both cases we have

$$\bigcap_{j\in\mathbb{Z}}(\mathbb{Z}_\beta/\beta^j) = \{0\}, \quad \overline{\bigcup_{j\in\mathbb{Z}}(\mathbb{Z}_\beta/\beta^j)} = \mathbb{R}.$$

The resulting decompositions of the two-dimensional cases are then straightforward. In cases 1 and 2 we introduce the following notation.

$$\mathcal{G}_j = \begin{cases} \Gamma_\beta/\beta^j & \text{(case 1)} \\ \widetilde{\Gamma}_\beta/\beta^j & \text{(case 2)} \end{cases}$$

and the sequence $(\mathcal{G}_j)_{j\in\mathbb{Z}}$ has the nested self-similarity

$$\ldots \subset \mathcal{G}_{j-1} \subset \mathcal{G}_j \subset \mathcal{G}_{j+1} \subset \ldots \subset \mathbb{Z}[\zeta] \tag{14}$$

with $j \in \mathbb{Z}$. In the internal space, we deduce from equations (10) and (11) that

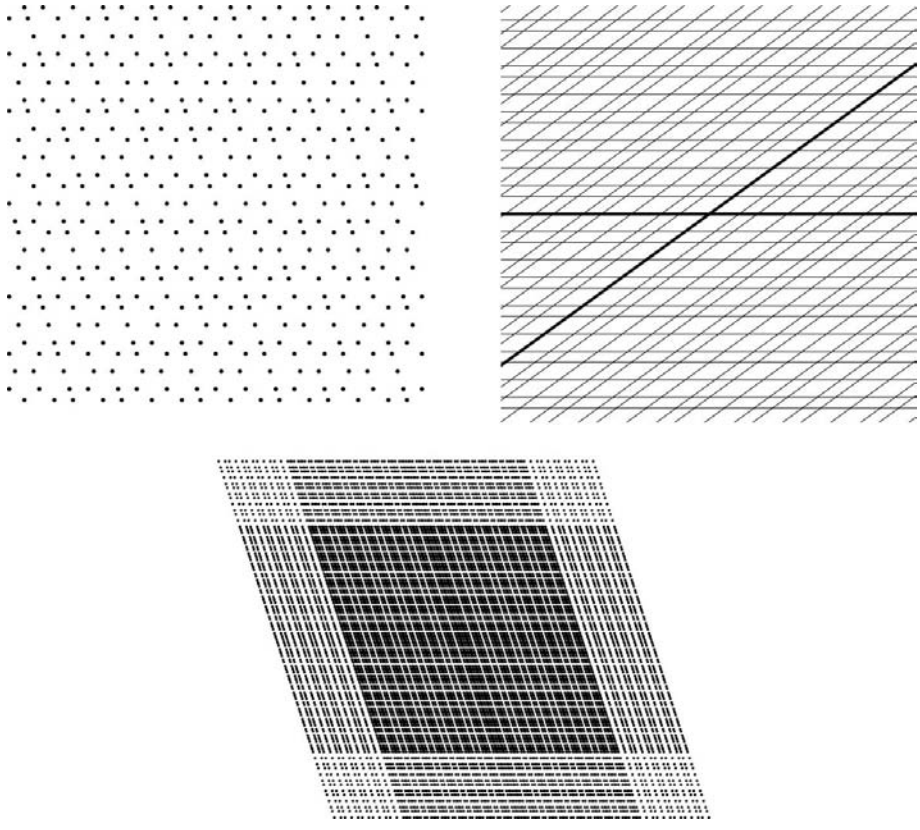

Figure 1
The τ-lattice Γ_τ, $\tau = (1 + 5^{1/2})/2$, with points (top left), and its trivial tiling made by joining points along the horizontal axis and along the direction defined by ζ (top right). The set (Galois-)conjugate to Γ_τ is shown below.

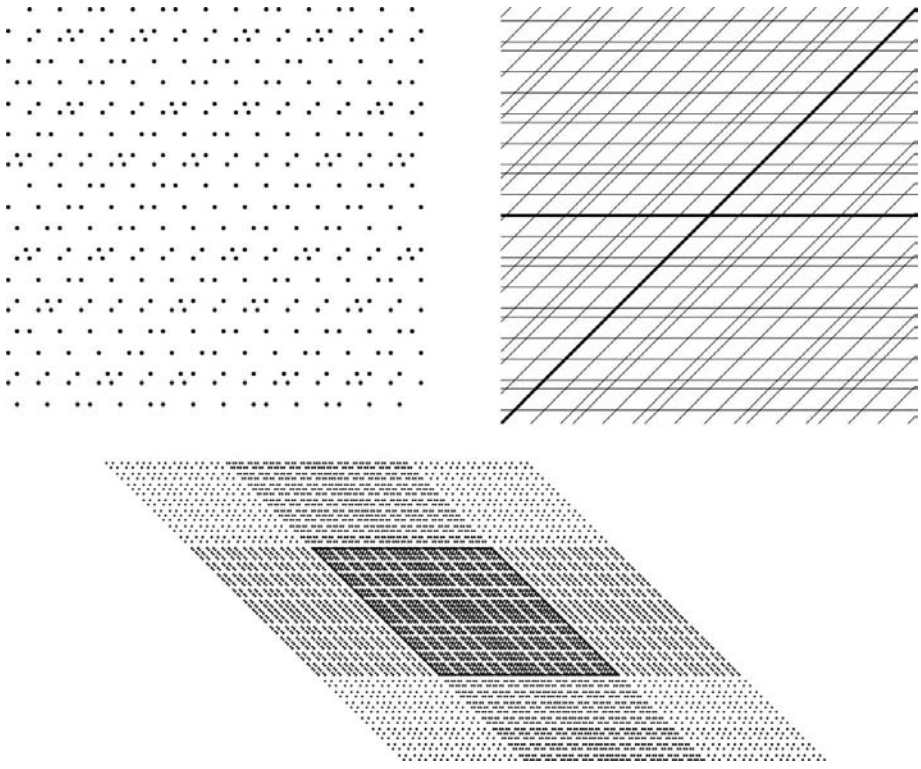

Figure 2
The δ-lattice Γ_δ, $\delta = 1 + 2^{1/2}$, with points (top left), and its trivial tiling obtained by joining points along the horizontal axis and along the direction defined by ζ (top right). The set (Galois-)conjugate to Γ_δ, *i.e.* its image in the 'internal' space, is shown below.

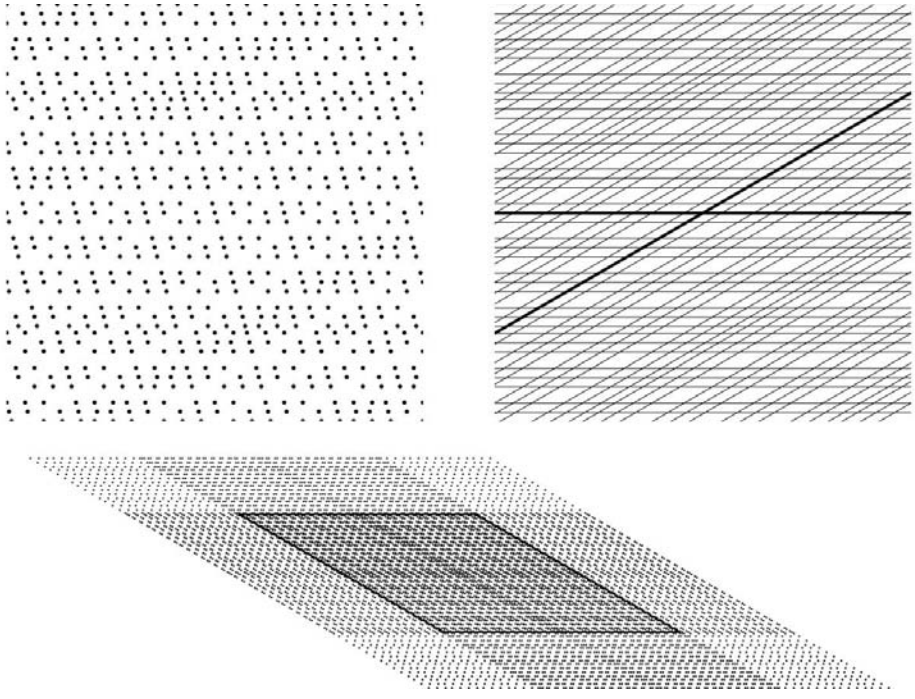

Figure 3
The decorated θ-lattice $\widetilde{\Gamma}_\theta$, $\theta = 2 + 3^{1/2}$, with points (top left), and its trivial tiling obtained by joining points along the horizontal axis and along the direction defined by ζ (top right). The set (Galois-)conjugate to Γ_θ is shown below.

$$\mathbb{Z}[\zeta] \cap \beta^j R_\beta = \mathcal{G}'_j \cap \beta^j R_\beta,$$

leading to

$$\lim_{j\to\infty} \mathcal{G}_j = \mathbb{Z}[\zeta]. \tag{15}$$

4. Cut-and-project sets and β-lattices

4.1. Algebraic filtering through β-lattices

Let us explore the details of the algebraic filtering algorithm, or algebraic sieving, used to construct an aperiodic set. Such an algorithm was introduced by de Bruijn (1981*a*,*b*) and was nicely applied by Moody & Patera (1994). It is the algebraic version of the cut-and-project method. This method was applied to the construction of cut-and-project sets on β-lattices by Barache *et al.* (1998).

The filtering procedure, possibly involving a 'phason' shift $\Phi \in \mathbb{C}$, reads

$$\Sigma^\Omega_\Phi = \{z \in \mathbb{Z}[\zeta] \mid z' - \Phi \in \Omega\} \tag{16}$$

$$= (\mathbb{Z}[\zeta] \cap (\Omega + \Phi))', \tag{17}$$

where Ω, a bounded subset of the plane, is the acceptance window of Σ^Ω_Φ. In the present article we study the diffraction patterns of aperiodic sets that are left invariant under the phasonic transforms Φ (Levine & Steinhardt, 1986). We shall then omit such transforms in the following. It follows from equations (10) and (11) that, for any $\Omega \subset R_\beta$, the associated model set Σ^Ω is a subset of $\mathcal{G}_0$.

There is an extensive literature on cut-and-project sets (also called model sets) and on their relation with their windows [see Moody (1997) for an overview]. The local symmetries of cut-and-project sets are closely related to the symmetries of their windows Ω. For example, for $\beta = \tau$, when Ω is a pentagon, the resulting model set admits local pentagonal symmetries. We shall then speak of a pentagonal set and so on. Recall at this point that one needs to sieve through specific β-lattices in order to obtain sets of given symmetries. Namely:

(i) pentagonal, decagonal and Penrose sets are sieved through τ-lattices and γ-lattices,

(ii) octagonal sets are sieved through δ-lattices, and

(iii) dodecagonal sets are sieved through θ-lattices.

The algebraic construction of (standard or singular) Penrose point sets is described in Appendix *D*.

4.2. Weighted Dirac measures supported by β-lattices

We now consider the weighted Dirac measure μ on Γ_β,

$$\mu = \sum_{z\in\Gamma_\beta} w(z)\delta_z.$$

The notion of measure with support in a β-lattice Γ_β is particularly convenient, since by properly choosing the weight function we can construct any kind of aperiodic set supported by Γ_β, particularly those sets which have quasicrystalline (QC) rotational symmetry. In this section we introduce the various weight functions that were used to perform this study.

4.2.1. Cut-and-project sets. Let Σ^Ω be a model set embedded in Γ_β. The weight function defined on Σ^Ω is given by

$$\begin{cases} w(z) = 1, & z' \in \Omega \\ w(z) = 0, & z' \notin \Omega \end{cases}$$

for all $z \in \Gamma_\beta$. It appears that for model sets we can abusively assert that the weight function in the physical space is the 'Galois conjugate' of the characteristic function of the window Ω in the internal space.

4.2.2. Functional window set. Let $\varphi : \mathbb{R}^2 \mapsto [0, 1]$ be a rapidly decreasing function centered at the origin. Define the weight function w of the weighted set Σ^φ, with slight misuse of notation, supported by Γ_β, by

$$w(z) = \varphi(z')$$

for all $z \in \Gamma_\beta$. This is a quite direct generalization of the notion of a window, where the weight function of the set is traditionally the characteristic function of the window.

For example, if φ is the Gaussian function $\exp(-|z|^2/\sigma^2)$, the weight function is then

$$w(z) = \exp[-(|z'|/\sigma)^2].$$

We can further combine the characteristics of a model set Σ^Ω and a functional windowed set by truncating the function φ along the edges of the window Ω. If χ_Ω is the characteristic function of Ω, the window is then $\varphi\chi_\Omega$ and the set is denoted $\Sigma^{\varphi\chi_\Omega}$.

4.2.3. Random window set. We now consider aperiodic sets admitting disorder. The principle of the method used here is to translate the window randomly during the filtering algorithm of the β-lattice, *i.e.* every time we test whether the conjugate z' of a particular point $z \in \Gamma_\beta$ is in or out of the window Ω, the latter is randomly translated. We could imagine that this model is the consequence of some thermal disorder. Concretely, this method generates aperiodic sets admitting uncorrelated phasons.

Let $\Phi \in \mathbb{C}$, and let $\Omega(\Phi)$ be the set given by

$$\Omega(\Phi) = \Phi + \Omega = \{u \in \mathbb{C} \mid u + \Phi \in \Omega\}$$

with $\Omega \subset \mathbb{C}$ a bounded set. If we let Φ assume random values such that $|\Phi| \in [0, |\Phi_{\max}|]$ during the filtering algorithm, the weight function of the aperiodic set $\Sigma^{\Omega(\Phi)}$ is given by

$$\begin{cases} w(z) = 1, & z' \in \Omega(\Phi) \\ w(z) = 0, & z' \notin \Omega(\Phi). \end{cases}$$

We can randomize functional windowed sets as well by defining the weight function of the sets Σ^φ by

$$w(z) = \varphi(z' - \Phi)$$

with Φ assuming random values such that $|\Phi| \in [0, |\Phi_{\max}|]$ during the filtering algorithm.

In Fig. 4 we display a random set built from a randomly translated decagonal window during the sieving algorithm.

5. Multiresolution analysis through β-lattices: general framework

Suppose that the pure point diffraction spectrum Π of a quasicrystal is supported by the (dense) point set Λ^* and the latter is the inductive limit of the nested sequence

$$\ldots \subset \mathcal{G}_{j-1} \subset \mathcal{G}_j \subset \mathcal{G}_{j+1} \subset \ldots \underset{\text{ind}}{\rightarrow} \Lambda^*. \tag{18}$$

Let us consider the diffraction spectrum $\Pi(X) \subset \Pi$, with a cutoff $X > 0$, given by

$$\Pi(X) = \{p = (x, I_x) \in \Pi \mid I_x \geq X\}.$$

It immediately follows from this definition that the set-valued function $X \mapsto \Pi(X)$ is 'decreasing' in the sense

$$X \geq Y \Rightarrow \Pi(X) \subset \Pi(Y)$$

until reaching the empty set value

$$X > I_{\max} \Rightarrow \Pi(X) = \{\emptyset\}.$$

Moreover, recall that when the diffractive structure is a cut-and-project set, which is the basic model of a quasicrystalline structure, then the set $\Pi(X)$ is supported by another cut-and-project set (Meyer, 1995). Thus, it is fairly reasonable for both the mathematical models and the physical structures to assume (within the context of the present paper based on the quadratic cyclotomic PV units) that for any $X \in \mathcal{I}$ there exists $j \in \mathbb{Z}$ such that $\Pi(X)$ has its support included in the point set $\mathcal{G}_j$. Supported means that for any pair $(x, I_x) \in \Pi(X)$, the spatial component x belongs to $\mathcal{G}_j$, and we shall write

$$\text{Supp}(\Pi(X)) \subset \mathcal{G}_j,$$

where, in general, the inclusion is strict. In order to convince the reader further of the suitability of β-lattices for reading diffraction patterns, we show in Fig. 5 the embedding of an experimental diffraction pattern into a τ-lattice. Note that this embedding was almost immediate.

Now we assume that to any $j \in \mathbb{Z}$ there corresponds a positive real number X_j defined by

$$X_j = \min\{X \mid \text{Supp}(\Pi(X)) \subset \mathcal{G}_j\}. \tag{19}$$

In other words, if $X \geq X_j$, then $\text{Supp}(\Pi(X)) \subset \mathcal{G}_j$, whereas if $X < X_j$, then there exists a $p = (x, I_x) \in \Pi(X)$ such that $x = x(p) \notin \mathcal{G}_j$. Again, this minimum is determined experimentally, since in practical implementation we deal with finite samples.

We are now in a position to introduce two partitions of the pure point diffraction pattern Π, induced by the nested sequence $(\mathcal{G}_j)_{j\in\mathbb{Z}}$. We shall indeed use $(\mathcal{G}_j)_{j\in\mathbb{Z}}$ as a multiresolving filter. Denote by P_0 and by G_0 the sets

$$P_0 = \Pi(X_0),$$
$$G_0 = \{p = (x, I_x) \in \Pi \mid x \in \mathcal{G}_0\}.$$

The set G_0 is the set of Bragg peaks supported by $\mathcal{G}_0$, whereas P_0 is the set of Bragg peaks supported by $\mathcal{G}_0$ of intensity greater than (or equal to) the cutoff X_0, as defined in equation (19). In the same fashion denote by P_1 and by G_1 the sets

$$P_1 = \Pi(X_1),$$
$$G_1 = \{p = (x, I_x) \in \Pi \mid x \in \mathcal{G}_1\}.$$

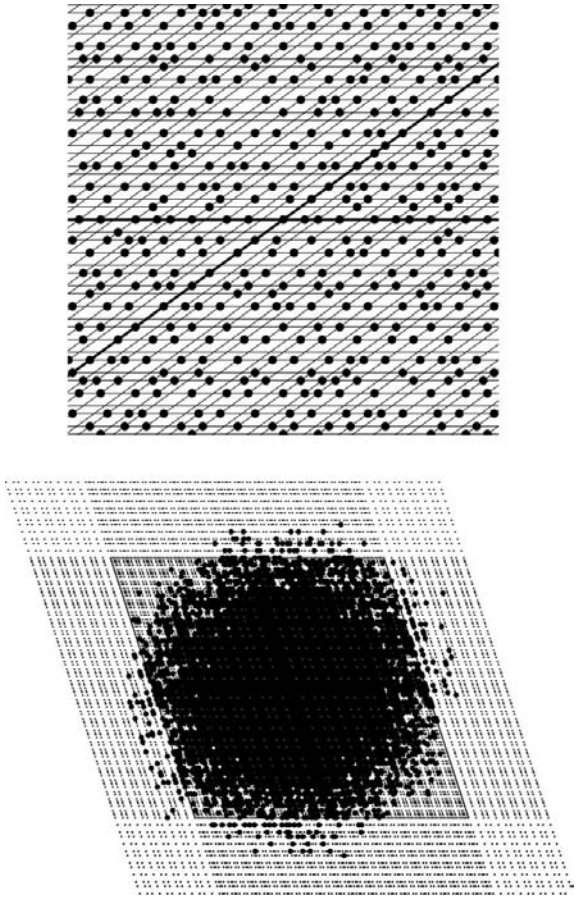

Figure 4
A 'decagonal' random set: in physical space (above) and in internal space (below).

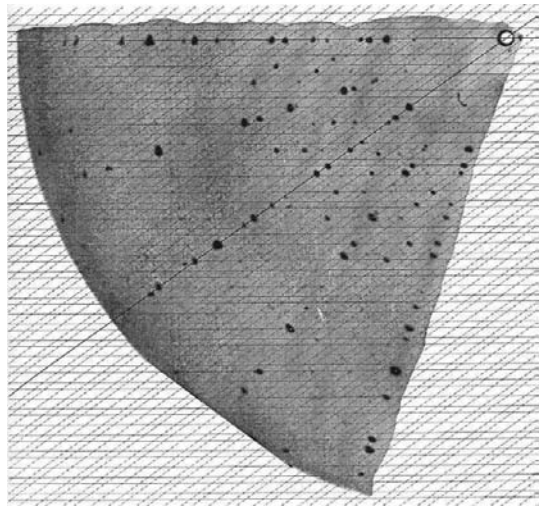

Figure 5
A monochromatic X-ray diffraction pattern ($Al_{63}Cu_{17.5}Co_{17.5}Si_2$, synchrotron LURE, Orsay) embedded in a τ-lattice at a suitable scale and orientation.

We obviously have $P_0 \subset P_1$ and $G_0 \subset G_1$. From here, we extend the decomposition to all $i, j \in \mathbb{Z}$, $(P_i)_{i\in\mathbb{Z}}$ and $(G_j)_{j\in\mathbb{Z}}$ as

$$P_i = \Pi(X_i), \tag{20}$$

$$G_j = \{p = (x, I_x) \in \Pi \mid x \in \mathcal{G}_j\} \tag{21}$$

obeying

$$\ldots \subset P_{i-1} \subset P_i \subset P_{i+1} \subset \ldots \subset \Pi,$$
$$\ldots \subset G_{j-1} \subset G_j \subset G_{j+1} \subset \ldots \subset \Pi.$$

Clearly, both increasing sequences have the pure point diffraction pattern as the inductive limit

$$\bigcup_{i\in\mathbb{Z}} P_i = \Pi,$$
$$\bigcup_{j\in\mathbb{Z}} G_j = \Pi.$$

Remark 1. Note that the decomposition of Π generated by the sequence $(G_j)_{j\in\mathbb{Z}}$ depends only on the geometrical discrete approximations to the ring $\mathbb{Z}[\zeta]$, *i.e.* the support of Π, provided by the sequence $(\mathcal{G}_j)_{j\in\mathbb{Z}}$. On the other hand, the decomposition of Π generated by the sequence $(P_i)_{i\in\mathbb{Z}}$ combines both geometrical and intensity features.

Denote now by D_1^P the complement of P_0 in P_1, and by D_1^G the complement of G_0 in G_1:

$$\begin{aligned} D_1^P &= P_1 \setminus P_0 \\ &= \{p = (x, I_x) \in \Pi \mid X_1 \leq I_x < X_0\}, \\ D_1^G &= G_1 \setminus G_0 \\ &= \{p = (x, I_x) \in \Pi \mid x \in \mathcal{G}_1 \setminus \mathcal{G}_0\}. \end{aligned}$$

More generally, the complement of P_i in P_{i+1} and the complement of G_j in G_{j+1} are given by

$$D_{i+1}^P = \{p = (x, I_x) \in \Pi \mid X_{i+1} \leq I_x < X_i\},$$
$$D_{j+1}^G = \{p = (x, I_x) \in \Pi \mid x \in \mathcal{G}_{j+1} \setminus \mathcal{G}_j\}.$$

Of course we have

$$P_{i+1} = P_i \cup D_{i+1}^P,$$
$$G_{j+1} = G_j \cup D_{j+1}^G.$$

Remark 2. In the language of wavelets and multiresolution analysis, the sets P_i and G_j are referred to as the tendency at scale i and j, respectively, and the sets D_{i+1}^P and D_{j+1}^G as the sets of details.

Iterating the above equations we obtain

$$P_i = \bigcup_{l=-\infty}^{i} D_l^P, \tag{22}$$

$$G_j = \bigcup_{k=-\infty}^{j} D_k^G. \tag{23}$$

Hence we get, at the limit, two distinct partitions of the pure point diffraction spectrum,

$$\Pi = \bigcup_{i=-\infty}^{\infty} D_i^P, \tag{24}$$

$$\Pi = \bigcup_{j=-\infty}^{\infty} D_j^G. \tag{25}$$

These two partitions are not identical and each one presents its own advantages in carrying out a classification of the Bragg peaks based on multiresolution. Let us profit from their coupled existence to refine this multiresolution procedure. The refinement is just based on the intersection of the two partitions. More precisely, we have the following resulting partition of the pure point diffraction spectrum:

$$\Pi = \bigcup_{i,j=-\infty}^{\infty} R_{i,j} \tag{26}$$

with

$$\begin{aligned} R_{i,j} &= D_i^P \cap D_j^G \\ &= \{p = (x, I_x) \in \Pi \mid x \in \mathcal{G}_j \setminus \mathcal{G}_{j-1},\ X_i \leq I_x < X_{i-1}\}. \end{aligned}$$

6. Multiresolution analysis through β-lattices: implementation

After this quite formal description of the partition of an aperiodic set diffraction pattern, we wish to implement this partition in order to analyze and to classify various structures. In this section we give guidelines for diffraction-pattern analysis through equations (26) and the equations below, using β-lattices. Our (numerical) explorations have an essentially pragmatic and illustrative character.

6.1. Approximations and computation

Denote by Λ an aperiodic set and by μ the weighted Dirac measure it supports, $\mu = \sum_{\lambda\in\Lambda} w(\lambda)\delta_\lambda$. We would like to analyze the function given by equation (2). We are then led to compute

$$I_k^{(L)} = \left| [1/\mathrm{Card}(\Lambda_L)] \sum_{\lambda\in\Lambda_L} w(\lambda) \exp(ik\lambda) \right|^2.$$

Recall that Λ_L is the restriction of Λ to a disc of radius L or some other bounded region of linear size L. When L is large enough, this approximation is relevant to the analysis of the diffraction pattern of Λ. We now need to determine the support of $I_k^{(L)}$, *i.e.*, the set of wavevectors k on which we compute $I_k^{(L)}$. Ideally this support should be, up to a scaling factor, the dense cyclotomic ring $\mathbb{Z}[\zeta]$ in the context of the present study, but we need to take an approximation of $\mathbb{Z}[\zeta]$. This approximation is naturally given by a dense enough β-lattice $\mathcal{G}_J$, for a finite fixed J (see below), which is embedded in $\mathbb{Z}[\zeta]$. Once again, if J is large enough, we consider this approximation relevant for our purpose. Hence we can consider as a good approximation the computation of the finitely supported distribution

$$I_J^{(M)} = \sum_{k \in \mathcal{G}_J^{(M)}} I_k^{(L)} \delta_k,$$

which is the restriction of the Fourier transform of the autocorrelation measure of μ to $\mathcal{G}_J^{(M)}$, where $\mathcal{G}_J^{(M)}$ denotes the restriction of the β-lattice $\mathcal{G}_J$ to the disc of radius M.

Switching to the notations we have adopted in this article, we see that $I_J^{(M)}(k)$ is equivalent to the set $\Pi_J^{(M)} = \{p = (k, I_k) \in \Pi \mid k \in \mathcal{G}_J^{(M)}\}$. We then choose a cutoff ϵ such that we discard all Bragg peaks of intensity smaller than ϵ. Eventually we obtain the set

$$\Pi_J^{(M)}(\epsilon) = \{p = (k, I_k) \in \Pi \mid k \in \mathcal{G}_J^{(M)},\ I_k \geq \epsilon\} \qquad (27)$$

of Bragg peaks supported by $\mathcal{G}_J^{(M)}$ and of intensities greater than or equal to ϵ. In summary, after fixing the quadruple (L, J, M, ϵ) of approximation parameters, we consider the set $\Pi_J^{(M)}(\epsilon)$, or $\Pi(\epsilon)$ for short, as the kind of realistic diffraction pattern one would obtain through experiment or traditional numerical computation, such as the one in Fig. 5.

6.2. The question of orientation of β-lattices

One important point has to be made precise here about the choice of orientation in the plane for the β-lattices $\mathcal{G}_j$ of the multiresolution sequence (actually, the choice for one of them), besides the fact that all of them are centered at the peak of maximal intensity. For the diffraction pattern of mathematical structures (β-lattices and their subsets obtained through the cut-and-project method, or variants of it, such as a Penrose set), the choice of orientation is determined by the original structure, as defined algebraically. For the Fourier transform of such a set, we represent Bragg peaks as they are determined by their computed coordinates in the plane. For experimental patterns, like the one in Fig. 5, two parameters of the quadruple (L, J, M, ϵ) are immediately fixed by the size M of the pattern and the cutoff ϵ determined by the distinguishable appearance of the peaks of weakest intensity. So the first task is to adjust simultaneously the scale J and the orientation, say θ, in order to include all the peaks (or at least the maximum number of peaks) into the set of nodes of the corresponding $\mathcal{G}_J^{(M)}(\theta)$. If, by chance, there are several such θ's, the multiresolution analysis should be carried out for each of them, in order to provide the structure with as many fingerprints indexed by possible orientations, since the aim is to make the diffracting structure enter into a classification scheme and possibly guess the geometrical organization of it by comparison with the diffraction 'fingerprints' of mathematical models.

6.3. β-Lattice indexation of Bragg peaks

Before we go into the partitions of $\Pi(\epsilon)$, we would like to index all Bragg peaks of $\Pi(\epsilon)$. Recall that the cut-and-project-based method for Bragg-peak indexation makes use of as many Miller integer indices as there are dimensions in the higher-dimensional space. In order to index a Bragg peak in, say, a two-dimensional structure, we need four Miller indices when the Pisot number involved in the structure is quadratic.

On the other hand, β-lattices offer an original indexing method, which allows only three integer indices to be used. Note, however, that both methods are equivalent.

The scale J is fixed such that $\mathcal{G}_0^{(M)}$ supports only the central Bragg peak in the restriction of the diffraction pattern on the disc of radius M. A Bragg peak $p = (k, I_k)$ is indexed by

$$p = (k, I_k) \ \leftrightarrow\ (1/j) \times (m, n),$$

where m and n are the indices of the mth and nth β-integers, b_m and b_n, and where j is the scale of the β-lattice $\mathcal{G}_j^{(M)}$, $j = 0, \ldots, J$, at which this peak first appears. This means that k reads as

$$k = (b_m + b_n\zeta)/\beta^j,$$

supposing that either b_m/β^j or b_n/β^j is irreducible as a ratio, *i.e.* both cannot be written as b'_m/β^{j-1} and b'_n/β^{j-1}. In other words, $(m, n)/j$ are the integer coordinates of k on the grid $\mathcal{G}_j$ of first appearance, *i.e.* the position of the node which supports p in the numeration system defined by $\mathbb{Z}_\beta$ (or a decorated version of it):

$$\mathcal{G}_j = \mathbb{Z}_\beta/\beta^j + (\mathbb{Z}_\beta/\beta^j)\zeta, \quad k \notin \mathcal{G}_{j-1}.$$

In Fig. 6, we represent ten Bragg peaks from the diffraction pattern of a decagonal structure (see below). The peaks are indexed as shown in Table 1.

Remark 3. The link between traditional indexing methods and the one we propose here is immediate. In standard quasicrystallographic methods, for two-dimensional structures, a Bragg peak is indexed by four integers $(q, r, s, t) \in \mathbb{Z}^4$, corresponding to its coordinates in the four-dimensional lattice within the cut-and-project framework, and we have

$$k = q + r\beta + (s + t\beta)\zeta.$$

β-Lattice formalism allows one to use only three integers to enclose information on the geometric localization, from the relations

$$q + r\beta = b_m/\beta^j, \quad s + t\beta = b_n/\beta^j.$$

Remark 4. Furthermore, self-similar properties of β-lattices, $\mathcal{G}_{j-1} \subset \mathcal{G}_j \subset \mathcal{G}_{j+1}$, allow one to get information on the set of wavevectors in a hierarchical way, depending on j.

6.4. Partitions of diffraction patterns

We now come to the two partitions of the diffraction pattern. The first reads

$$\Pi(\epsilon) = P_0 \cup \left(\bigcup_{i=1}^{J} D_i^P \right),$$

where we have fixed

$$D_J^P = \{p(k, I_k) \in \Pi(\epsilon) \mid \epsilon \leq I_k < X_{J-1}\}.$$

The second reads

Table 1
Indexed Bragg peaks in Fig. 6.

Intensity	m	n	j
0.983761	1	−1	1
0.983761	−1	1	1
0.983761	1	0	2
0.983761	0	1	2
0.983761	−1	2	2
0.983761	−2	1	2
0.983761	−1	0	2
0.983761	0	−1	2
0.983761	1	−2	2
0.983761	2	−1	2

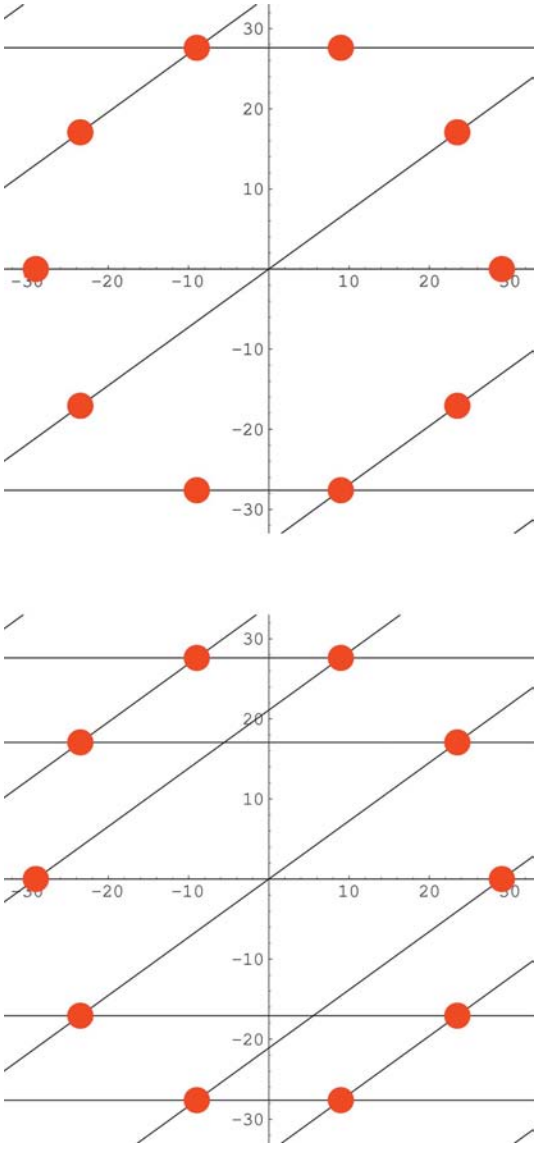

Figure 6
Ten Bragg peaks from the diffraction pattern of a decagonal structure. Above: the grid $\mathcal{G}_1$, in which only two peaks lie on nodes of the grid corresponding to $j = 1$; these two peaks are indexed by $(-1, 1)/1$ and $(1, -1)/1$. Below: the grid $\mathcal{G}_2$, in which we can embed the eight other peaks $(1, 0)/2$, $(-1, 0)/2$, ... Notice how the original tenfold symmetry is first reduced to a twofold symmetry before being restored.

$$\Pi(\epsilon) = G_0 \cup \left(\bigcup_{j=1}^{J} D_j^G \right),$$

where we have fixed

$$D_J^G = \{p(k, I_k) \in \Pi(\epsilon) \mid k \in \mathcal{G}_j \setminus \mathcal{G}_{j-1},\ I_k \geq \epsilon\}.$$

Note that, by convention, we put

$$P_0 = G_0 = \{p(k, I_k) \mid k = (0, 0),\ I_k = 1\}.$$

Eventually we obtain the partition

$$\Pi(\epsilon) = P_0 \cup \left(\bigcup_{i,j=1}^{J} R_{i,j} \right),$$
$$= P_0 \cup \left(\bigcup_{i,j=1}^{J} D_i^P \cap D_j^G \right).$$

Remark 5. Practically, most of the $R_{i,j}$ are empty, as we shall see in the numerical examples. Each sequence $(R_{i,j})_{0 \leq i,j \leq J}$ is characteristic of a class of diffractive structures. Hence the determination of the sequences (i, j) allows one to discriminate those classes of diffractive structures.

7. Numerical examples

We now implement the multiresolution analysis described above. As a first test of our method, we will restrict the trial to the fivefold and tenfold symmetries (for which τ or one of its powers only are involved as an inflation factor). We first apply our procedure to academic cases, in which the diffraction spectra are those of β-lattices or simple model sets defined by symmetric windows or randomly defined windows. Note that for certain of these mathematical models there exist exact formulae for the diffraction intensity (Gazeau & Verger-Gaugry, 2006). Nevertheless, we prefer here to stick to our 'experimental' approach for pedagogical and teaching reasons. The last section (§7.6) will be devoted to multiresolution analysis of the diffraction pattern of a QC model that has been established on experimental grounds (Steurer & Kuo, 1990*a*,*b*).

For each one of these spectra, we tabulate in Tables 2 to 12 the values assumed by $|R_{i,j}| \equiv \mathrm{Card}(R_{i,j})$ for $1 \leq i, j \leq J$. The value 1 corresponding to the central Bragg peak of maximal intensity, $I_{\max} = 1$, is also displayed in the top left corner, indexed by $i = 0, j = 0$.

Each sequence $(R_{i,j})_{0 \leq i,j \leq J}$ seems to be characteristic of a class of diffracting structures. Two-dimensional diffraction patterns can then be sorted into three general categories, depending on their similarities with the diffraction patterns of (1) a τ-lattice, (2) a decagonal model set or (3) a Penrose set.

This gives us a first overview of aperiodic structures and their classification.

In addition to the tables and for each i we show figures of the corresponding diffraction pattern $\Pi(X_i)$, with different

colors to help distinguish items belonging to elementary boxes $R_{i,j}$. Each figure is accompanied by its internal space counterpart.

7.1. The τ-lattice Γ_τ

We start our investigation of aperiodic sets with the diffraction-pattern analysis of the τ-lattice, Γ_τ. In Fig. 7, we display the diffraction pattern $\Pi_J^M(\epsilon)$. Note that the set of Bragg peaks 'rebuilds' the τ-lattice. This interesting fact appears more clearly in the internal space, where peaks place themselves uniformly within the convex hull $\tau^7 R_\tau$.

In Table 2 we display all Bragg peaks arising from the diffraction pattern of the structure, depending on their intensity and their scale. Recall that the set $R_{i,j}$ is the set of Bragg peaks whose intensities lie within $X_i \leq I < X_{i-1}$, and the positions of which belong to the grid $\mathcal{G}_j$ without belonging to the grid $\mathcal{G}_{j-1}$. Table 2 displays the number of diffraction peaks which belong to each subset $R_{i,j}$. The rows are the intensities X_i viewed as the minima of the finite samples considered. The columns are the scales j of the grids $\mathcal{G}_j = \Gamma_\tau/\tau^j$. In Figs. 8 and 9 we display the decomposition of the τ-lattice diffraction pattern in both physical space and internal space. For each set $R_{i,j}$, the peaks that belong to all lower-indexed sets $R_{i-1,j-1}, R_{i-2,j-2}, \ldots$ down to $R_{0,0}$ are represented by open circles. If two or more new sets are represented in the same figure, *e.g.* $R_{5,4}$ and $R_{5,5}$ in the lower part of Fig. 9, they are distinguished by different colors. Note that Bragg peaks progressively appear in clusters showing rotational symmetries (*e.g.* twofold, then tenfold...) at each step of this decreasing intensity process, despite the non-rotational invariance of the successive supports Γ_τ/τ^j. This important feature will occur again in all other explorations shown below.

7.2. Gaussian window set

This isotropic set is sieved on Γ_τ through the weight function

$$w(z) = \varphi(z') = \exp[-(|z'|/\sigma)^2],$$

where $\sigma = 1/\tau$. This means that the standard deviation of the Gaussian is chosen such that there is practically no truncation effect, see §4.2.2:

$$\Sigma^\varphi \cap \Gamma_\tau \simeq \Sigma^\varphi \cap \mathbb{Z}[\zeta].$$

We can even claim that it is 'neutral', in the sense that the sieving effect on the τ-lattice is not apparent.

The partition shown in Table 3 arises from the diffraction pattern shown in Fig. 10. The observations resulting from this example raise the question: why does an isotropic neutral set have a diffraction pattern closely related to the diffraction pattern of a τ-lattice? One can conclude without any doubt that the geometrical properties of both sets are closely related.

In fact, this observation supports the idea that τ-lattices might be accepted as an eligible universal frame in which we can study the properties of aperiodic constructions with fivefold or tenfold symmetries.

Table 2
Partition of the τ-lattice.

	j							
X_i	0	1	2	3	4	5	6	7
$X_0 = 1$	1							
$X_1 = 0.970673$		2						
$X_2 = 0.924877$			10					
$X_3 = 0.814151$				10				
$X_4 = 0.642199$					16			
$X_5 = 0.300888$					18	46		
$X_6 = 0.046841$						32	62	
$X_7 = 0.02$						2	32	12

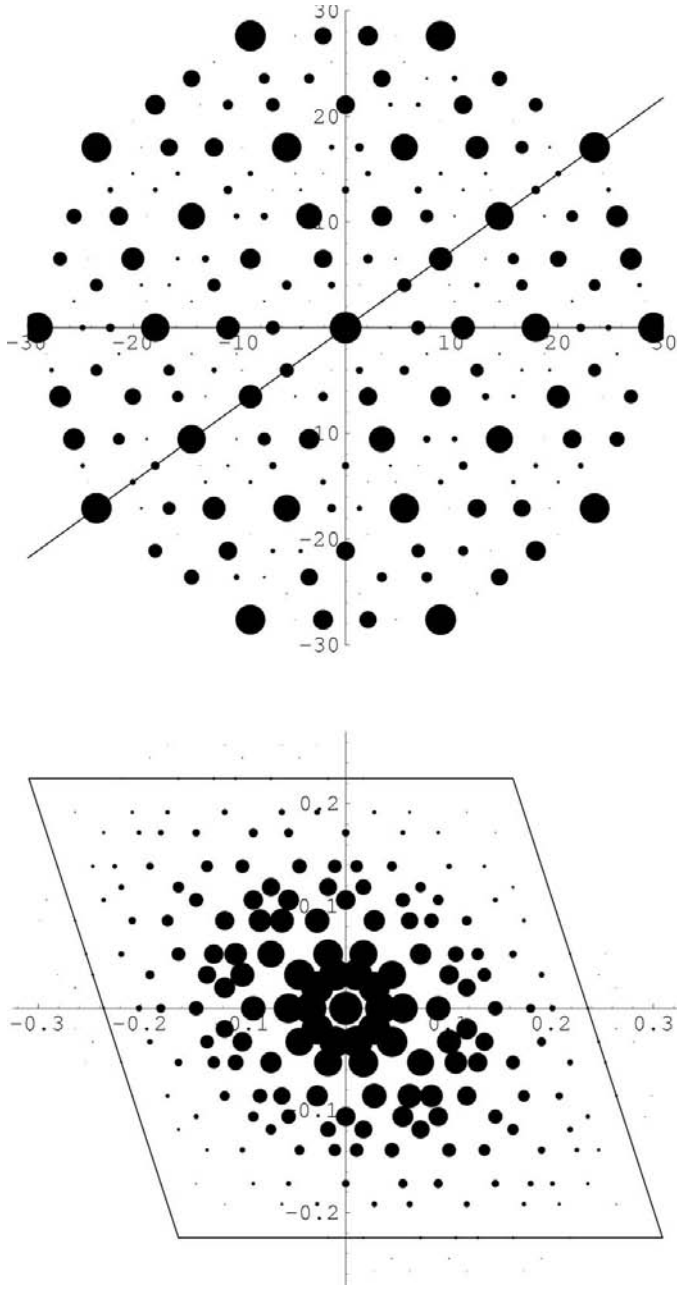

Figure 7
The diffraction pattern of the τ-lattice. Above: the physical space, along with the grid $\mathcal{G}_0$; below: the corresponding image in the internal space, along with the convex hull $\tau^7 R_\tau$.

7.3. Pentagonal and decagonal sets

Let us now turn to pentagonal and decagonal sets. They are examined together because their diffraction patterns are almost the same and can be included in the same category. Note that blank entries or rows in Tables 4 and 5 correspond to empty sets.

Once again, we have to go deep down into the intensities of the peaks to notice that the two distributions of Bragg peaks are different. Therefore, we may question the possibility of distinguishing between the two structures experimentally without a reference structure.

In Figs. 11 and 12, we show the partition of the diffraction pattern of a pentagonal set.

7.4. Penrose set

Penrose sets are a particular class of aperiodic sets. This is well illustrated by the fingerprint decompositions of their diffraction patterns. Recall that a Penrose set is formed by the union of four pentagonal sets. Each of these sets has a standard pentagonal set diffraction spectrum, like those just explored in the previous section, but their union, *i.e.* the Penrose set, does not.

In the following, we first give the partition of the diffraction pattern of the Penrose set (see Fig. 13). Then, in order to understand how the different constituent sets interact together, we display two different versions with alternative weight functions.

7.4.1. Diffraction of a Penrose set. Table 6 shows the distribution of Bragg peaks according to the multiresolution partition (Fig. 14). Note the four empty rows before reaching the secondary peaks. We can distinguish two parts. In the array we have a diagonal part and a horizontal part formed by the subsets $R_{8,1}, \ldots, R_{8,5}$. The diagonal part reminds one of the pentagonal diffraction-pattern partition (blank entries or rows correspond to empty sets). We can show that, up to a $\pi/10$ rotation and a dilation, it is possible to embed the support of $P(X_7)$ of the Penrose diffraction pattern into the pentagonal diffraction pattern. On the other hand $D^P(X_8)$, $P(X_8) = P(X_7) \cup D^P(X_8)$, cannot be embedded in it. We thus deduce that these two parts, *i.e.* $P(X_7)$ and $D^P(X_8)$, can be interpreted as a reminiscence of the pentagonal diffraction pattern and a set of satellite peaks.

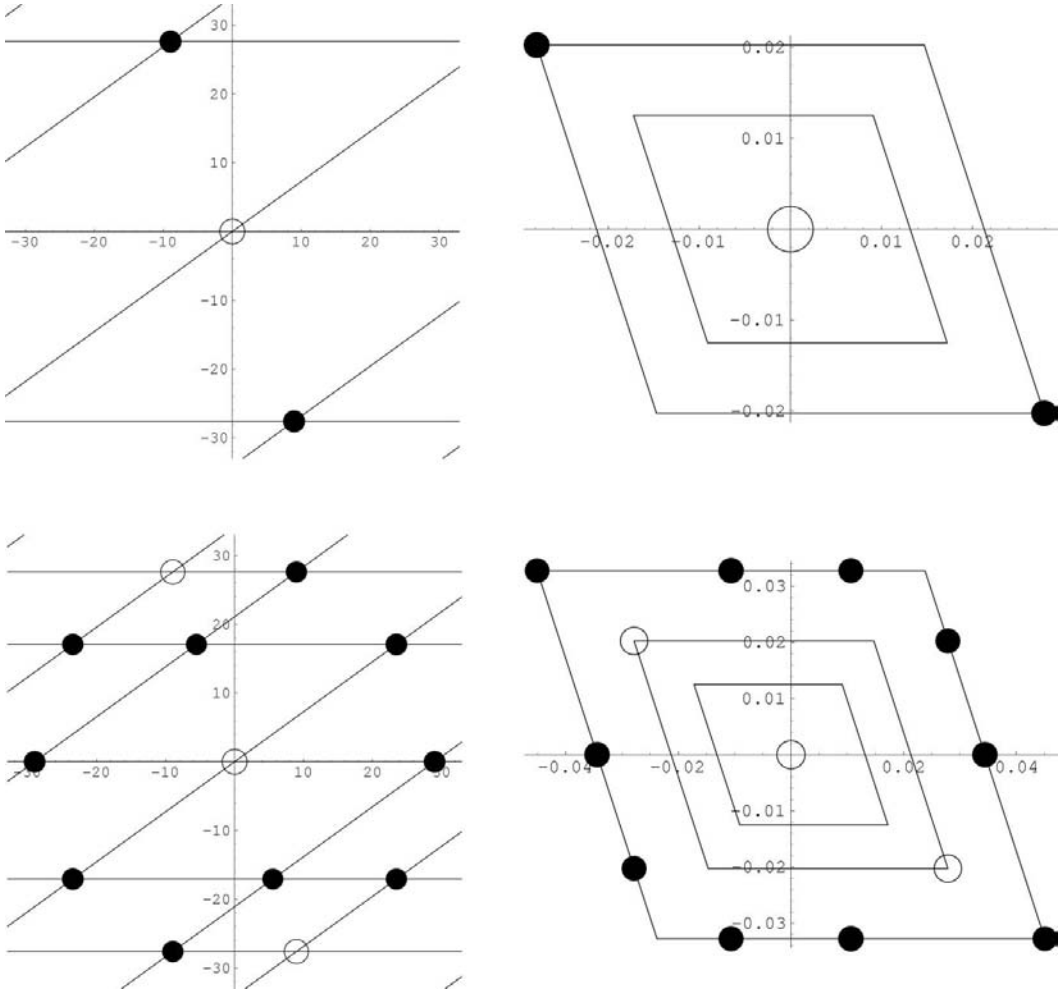

Figure 8
Partition of the τ-lattice diffraction pattern: $R_{1,1}$ (top) and $R_{2,2}$ (bottom). On the right the corresponding images in internal space are shown.

7.4.2. Penrose sets with alternative weight functions. We then chose to study two Penrose sets with different weight functions. Recall that the window of the Penrose set is composed of two small subwindows, Ω_1 and Ω_4, and two large subwindows Ω_2 and Ω_3.

First weight function:

$$w(\Omega_1) = 1, \quad w(\Omega_2) = 1/\tau, \quad w(\Omega_3) = 1/\tau, \quad w(\Omega_4) = 1.$$

This set gives rise to the partition shown in Table 7.

Second weight function:

$$w(\Omega_1) = 1/\tau, \quad w(\Omega_2) = 1, \quad w(\Omega_3) = 1, \quad w(\Omega_4) = 1/\tau.$$

This set gives rise to the partition shown in Table 8.

In the first pattern, the partition is roughly the same as in the standard Penrose set diffraction pattern. On the other

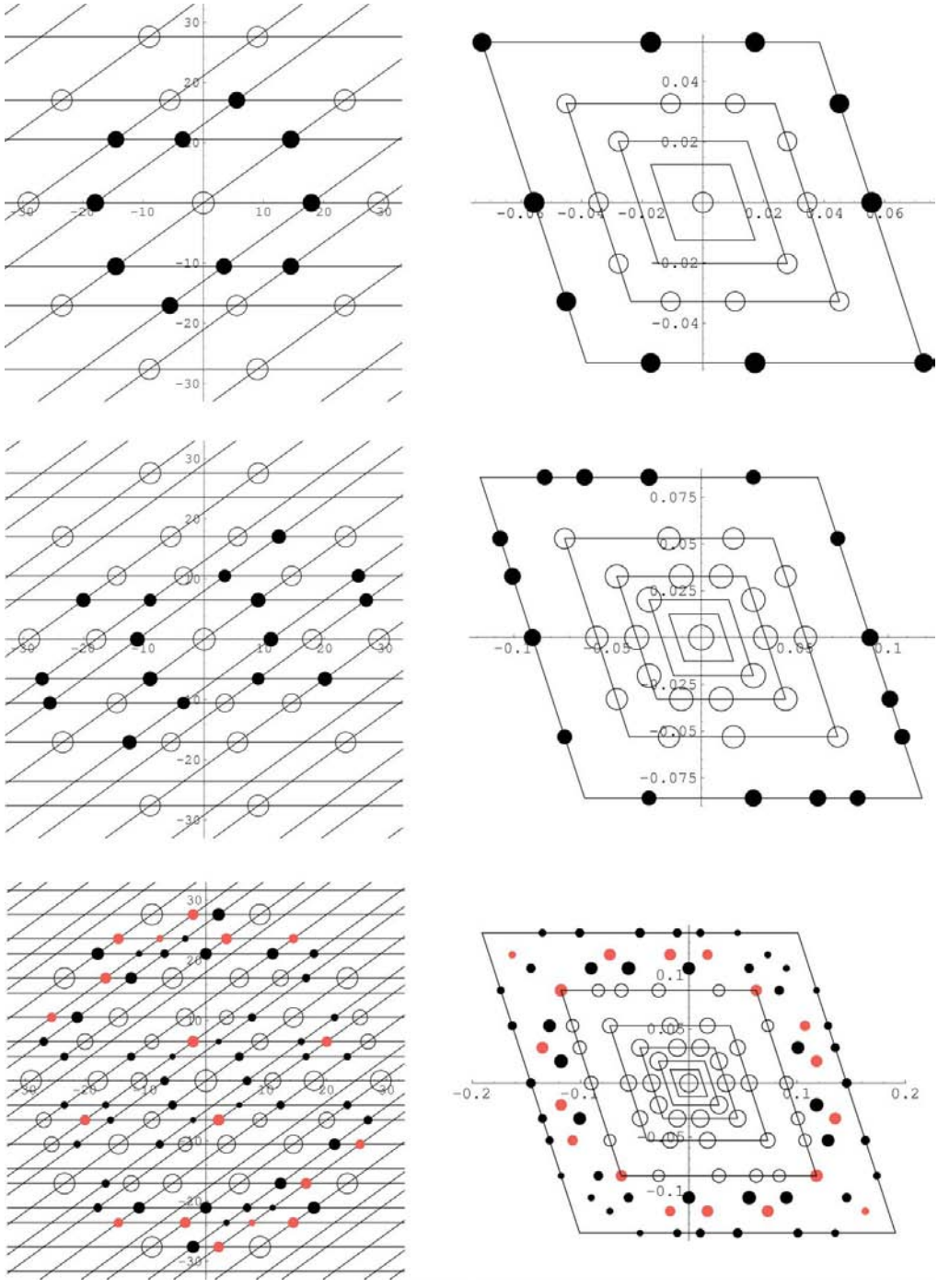

Figure 9
Partition of the τ-lattice diffraction pattern: $R_{3,3}$ (top), $R_{4,4}$ (middle), and $R_{5,4}$ and $R_{5,5}$ (bottom). On the right the corresponding images in internal space are shown.

Table 3
Partition of an isotropic neutral set.

	j							
X_i	0	1	2	3	4	5	6	7
$X_0 = 1$	1							
$X_1 = 0.965234$		2						
$X_2 = 0.911513$			10					
$X_3 = 0.78456$				10				
$X_4 = 0.715022$					12			
$X_5 = 0.415008$					20	42		
$X_6 = 0.156594$					2	28	56	
$X_7 = 0.02$						10	108	90

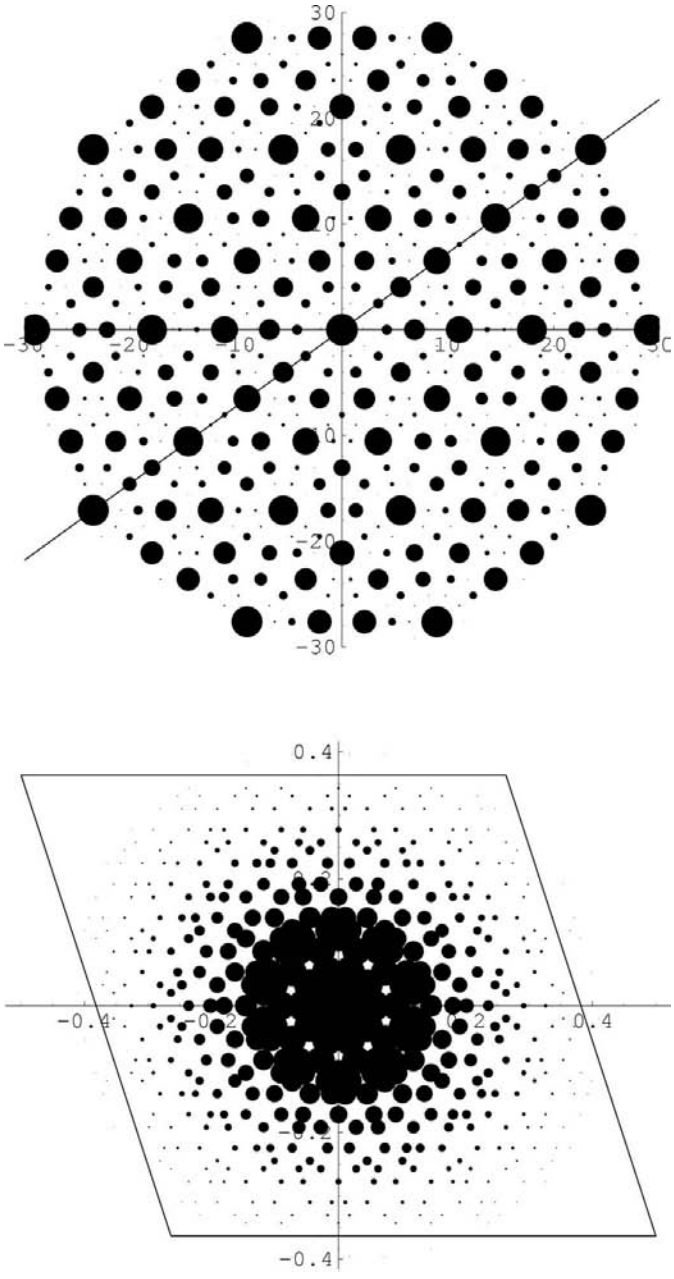

Figure 10
Above: the diffraction pattern of a Gaussian window set, with the grid $\mathcal{G}_0$. Below: the corresponding image in internal space, with the convex hull $\tau^7 R_\tau$.

hand, in the second pattern, the peaks are not distributed in the same fashion. Most of the satellite peaks remain in $P(X_8)$, but some of them appear in $P(X_7)$. Note that the intensity of the shifted peaks is somewhat high.

7.4.3. Individual windows. Let us now focus on individual windows of the Penrose set. As expected, the decompositions are standard pentagonal diffraction-pattern decompositions. They are shown for a large window in Table 9 and for a small window in Table 10.

7.5. Random window sets

In this section we display diffraction patterns of sets admitting disorder. The initial set is a pentagonal set, to which we progressively add disorder. We chose the following values for $\Phi_{\max} \in \{0.2, 0.4, 0.6, 0.8, 1\}$. The partition displayed in Table 11 is for $\Phi_{\max} = 0.2$ and the partition displayed in Table 12 is for $\Phi_{\max} = 1$. Once again, the conclusion is that it is not possible to distinguish such random sets from pentagonal or decagonal sets, except for a global intensity decay, as was the case for distinguishing pentagonal and decagonal sets (§7.3).

7.6. The model of Steurer and Kuo

We conclude this study by a brief overview of the analysis of the Steurer and Kuo model. The quasiperiodic atomic structure arising from this model was determined for the decagonal phase of nominal composition $Al_{65}Cu_{20}Co_{15}$ on the basis of X-ray diffraction experiments (Steurer & Kuo, 1990*a*,*b*; Fettweis, 1994; Fettweis *et al.*, 1995). The structure is constructed from the projection of a five-dimensional lattice: four dimensions are devoted to quasiperiodic planes; the fifth, which is perpendicular to the four others, represents the periodic direction. This allows the reciprocal lattice to be indexed with five indices.

Remark 6. As ascertained through Tables 13 to 16, there is quite a difference between the mathematical structures we have displayed so far and the present Steurer and Kuo physical model, refined on the basis of experimental data.

(1) Two-dimensional models are not directly adaptable to the $Al_{65}Cu_{20}Co_{15}$ structure. One should compute the diffraction pattern for the three-dimensional structure. The reason for this is that there exist constructive and destructive interferences between different diffracting planes, as we shall see below. In Tables 13 to 16, we give the partition of the diffraction pattern as derived from the moduli of the amplitudes of the peaks instead of their intensities.

(2) We have to take into account the atomic form factor, which depends on the wavevector **k** in an X-ray diffraction experiment.

7.6.1. The Steurer and Kuo model. The Steurer and Kuo model is composed of eight pentagonal windows in which are distributed the three elements of the AlCuCo alloy. The structure factor is given by

Table 4
Partition of a pentagonal set.

	j								
X_i	0	1	2	3	4	5	6	7	8
$X_0 = 1$	1								
$X_2 = 0.986523$		2	8						
$X_3 = 0.965038$			2	8					
$X_4 = 0.910641$				2	8				
$X_5 = 0.780226$					24	36			
$X_6 = 0.510066$					2	34	44		
$X_7 = 0.13773$						10	134	146	
$X_8 = 0.02$							36	146	108

Table 5
Partition of a decagonal set.

	j								
X_i	0	1	2	3	4	5	6	7	8
$X_0 = 1$	1								
$X_2 = 0.983761$		2	8						
$X_3 = 0.957952$			2	8					
$X_4 = 0.893036$				2	8				
$X_5 = 0.740135$					24	36			
$X_6 = 0.438388$					2	34	44		
$X_7 = 0.078671$						10	134	146	
$X_8 = 0.02$							24	86	40

$$F(\mathbf{k}) = (1/\Omega_{\rm tot}) \sum_{j=1}^{8} \exp(i2\pi\mathbf{k}\cdot\mathbf{r}_j)\tilde{F}_j(\mathbf{k}_\varphi)T_j(\mathbf{k}_\varphi, \mathbf{k}_t)g_j(\mathbf{k}_t). \quad (28)$$

The summation is taken over the eight different surfaces, indexed by $j = 1, \ldots, 8$. The notations correspond to the following elements:

(1) $\Omega_{\rm tot}$ is the total surface of all the eight windows. This normalization factor replaces the total number of atoms in a unit cell for structure-factor computation of a crystal.

(2) $\tilde{F}_j$ is the mean form factor for each window, considering occupation rates. We have

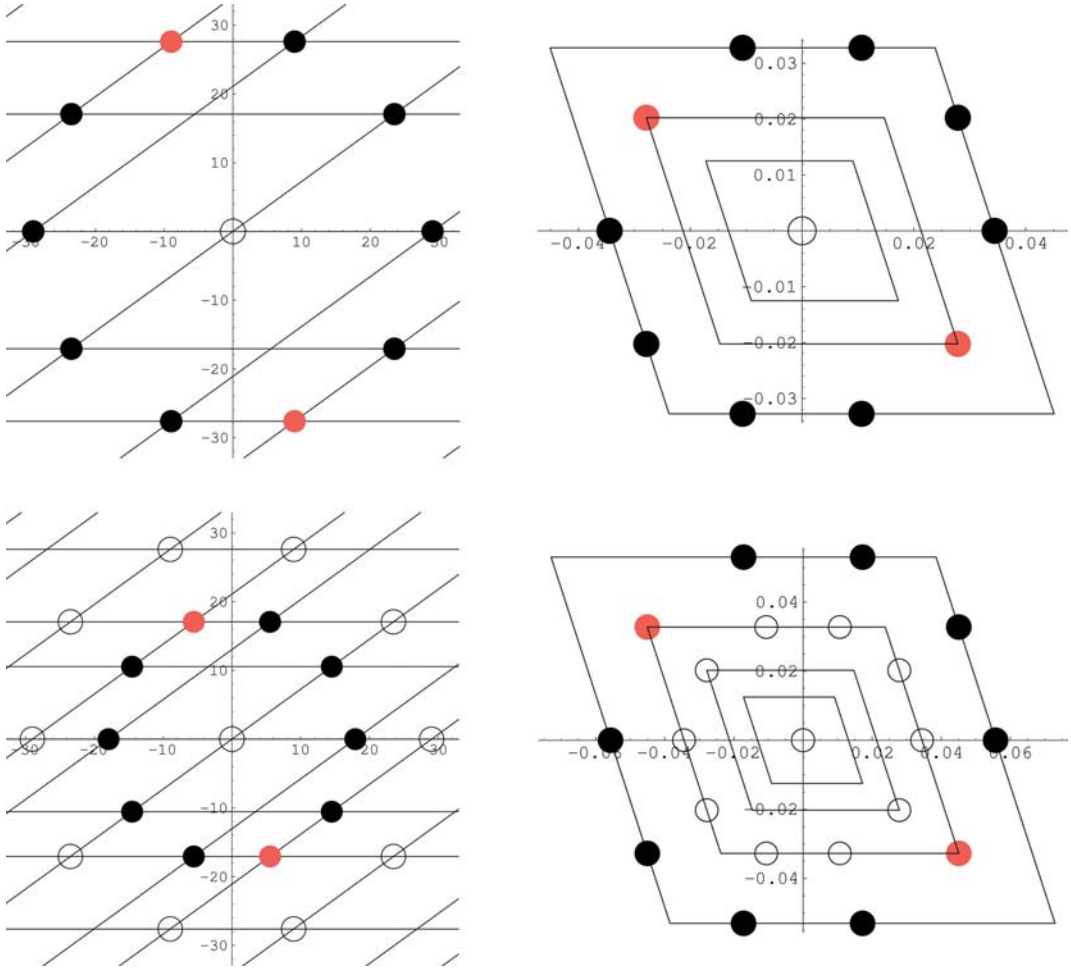

Figure 11
Pentagonal diffraction-pattern partition: top $R_{0,0}$, $R_{2,1}$ and $R_{2,2}$; bottom $R_{3,2}$ and $R_{3,3}$. Notice here and in the following figures to what extent the original tenfold symmetry is present at each step of the partition.

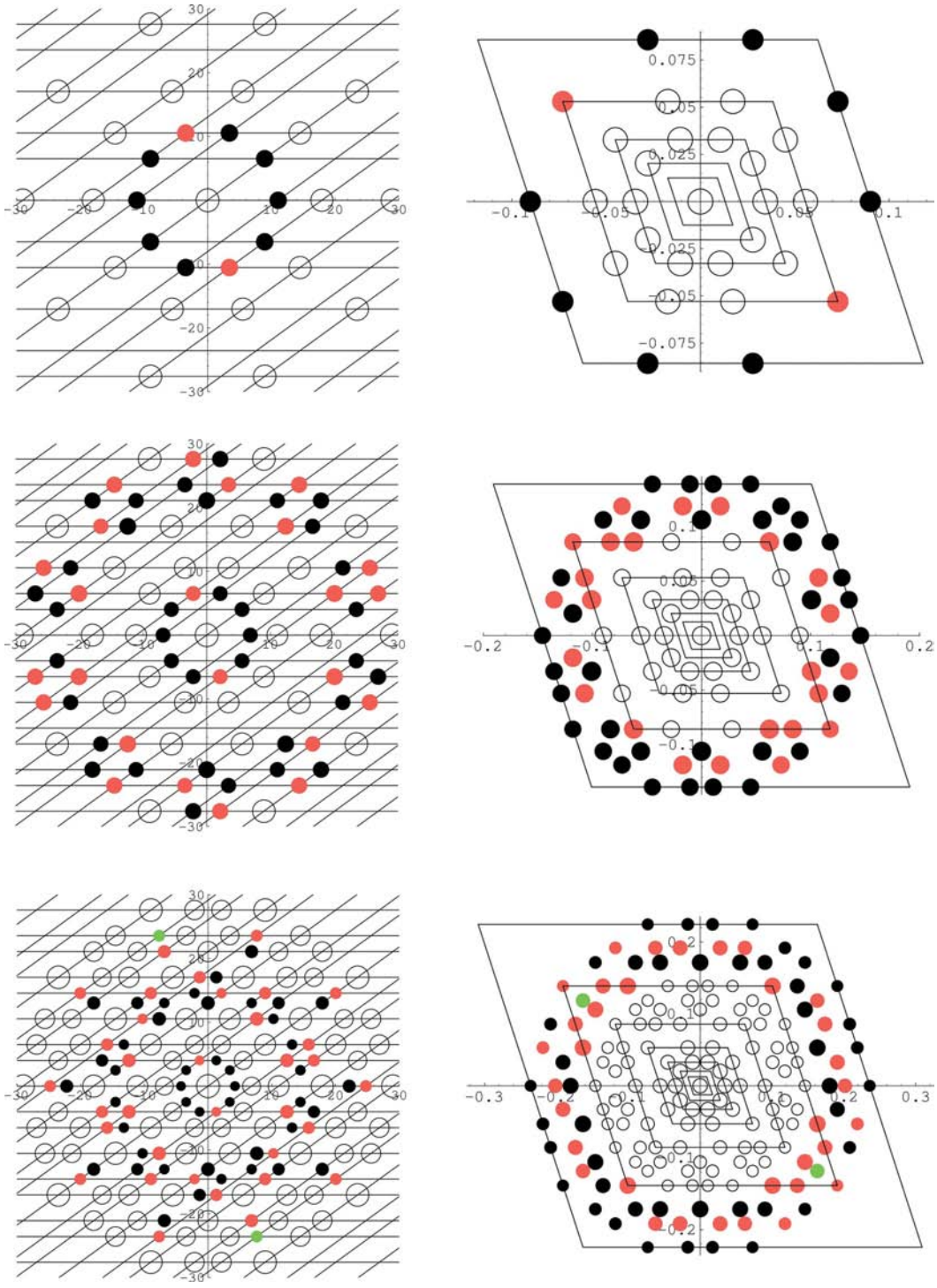

Figure 12
Pentagonal diffraction-pattern partition: top $R_{4,3}$ and $R_{4,4}$; middle $R_{5,4}$ and $R_{5,5}$; bottom $R_{6,4}$, $R_{6,5}$ and $R_{6,6}$.

$$\tilde{F}_j = p_j(p_j^{\mathrm{Al}} f_{\mathrm{Al}} + p_k^{\mathrm{MT}} f_{\mathrm{MT}}),$$

where

(*a*) p_j is the total occupation rate for window j;

(*b*) p_j^{Al} is the occupation rate for aluminium and f_{Al} is the form factor for aluminium;

(*c*) p_k^{MT} is the occupation rate for transition metals, *i.e.* cobalt or copper, and f_{MT} is the mean form factor of the two transition metals.[1]

(3) T_j is the Debye–Waller temperature factor.

[1] Their form factors are too close to be distinguishable during the experiment.

Table 6
Partition of a Penrose set.

	j									
X_i	0	1	2	3	4	5	6	7	8	9
$X_0 = 1$	1									
$X_5 = 0.92691$					6	4				
$X_6 = 0.757223$					2	14	4			
$X_7 = 0.378328$						5	34	34		
$X_8 = 0.038948$		2	8	2	12	34	86	136	90	
$X_9 = 0.02$							10	34	40	16

Table 7
Partition of a Penrose set with the first weight function.

	j									
X_i	0	1	2	3	4	5	6	7	8	9
$X_0 = 1$	1									
$X_5 = 0.932513$					6	4				
$X_6 = 0.774617$					2	14	4			
$X_7 = 0.412985$						2	34	34		
$X_8 = 0.060652$		2	8	2	12	34	42	66	74	
$X_9 = 0.02$							68	222	212	48

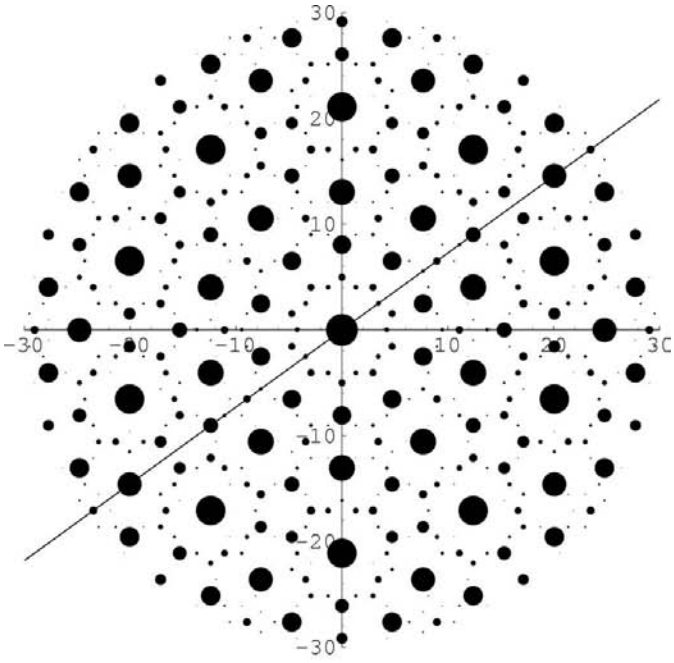

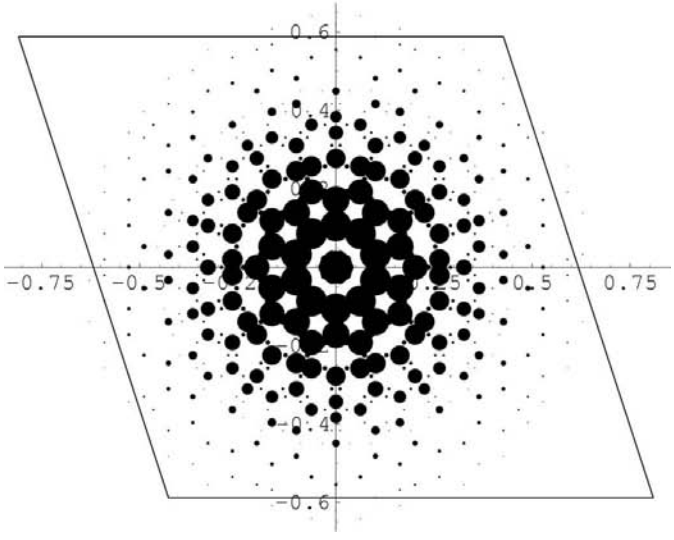

Figure 13
The diffraction pattern of a Penrose set.

Table 8
Partition of a Penrose set with the second weight function.

	j									
X_i	0	1	2	3	4	5	6	7	8	9
$X_0 = 1$	1									
$X_5 = 0.922402$					6	4				
$X_6 = 0.743338$					2	14	4			
$X_7 = 0.333604$		2	8	2	8	2	34	34		
$X_8 = 0.032751$					4	34	96	172	114	
$X_9 = 0.02$								18	24	8

Table 9
Partition of a Penrose set with a large window.

	j									
X_i	0	1	2	3	4	5	6	7	8	9
$X_0 = 1$	1									
$X_2 = 0.996369$		2	8							
$X_3 = 0.990517$			2	8						
$X_4 = 0.975333$				2	8					
$X_5 = 0.936498$					24	36				
$X_6 = 0.84088$					2	34	44			
$X_7 = 0.628119$						10	134	146		
$X_8 = 0.288875$							44	336	330	
$X_9 = 0.02$								106	820	694

Table 10
Partition of a Penrose set with a small window.

	j									
X_i	0	1	2	3	4	5	6	7	8	9
$X_0 = 1$	1									
$X_2 = 0.990432$		2	8							
$X_3 = 0.975114$			2	8						
$X_4 = 0.935947$				2	8					
$X_5 = 0.839592$					24	36				
$X_6 = 0.625628$					2	34	44			
$X_7 = 0.266554$						10	134	146		
$X_8 = 0.02$							42	300	258	

(4) $g_j(\mathbf{k}_t)$ is the geometrical structure factor, that is the Fourier transform of the window.

7.6.2. Multiresolution partition. We present the partition of the diagram for planes $l = 0$, $l = 1$, $l = 2$ and $l = 3$ in Tables 13, 14, 15 and 16, respectively. The corresponding diffraction patterns are shown in Figs. 15–18.

Remark 7. All the models previously considered in this paper had uniform structure factors. This is obviously not the case for the Steurer and Kuo model, where the factor decreases for large angles. Moreover, we have to consider interactions between the different chemical elements within the structure, see equation (28). Therefore, the partition we display here can only be considered as a trial (blank boxes or rows correspond to empty sets). We shall not try to derive physical properties from it.

On the other hand, we wish to take this study further in order to refine the multiresolution partition.

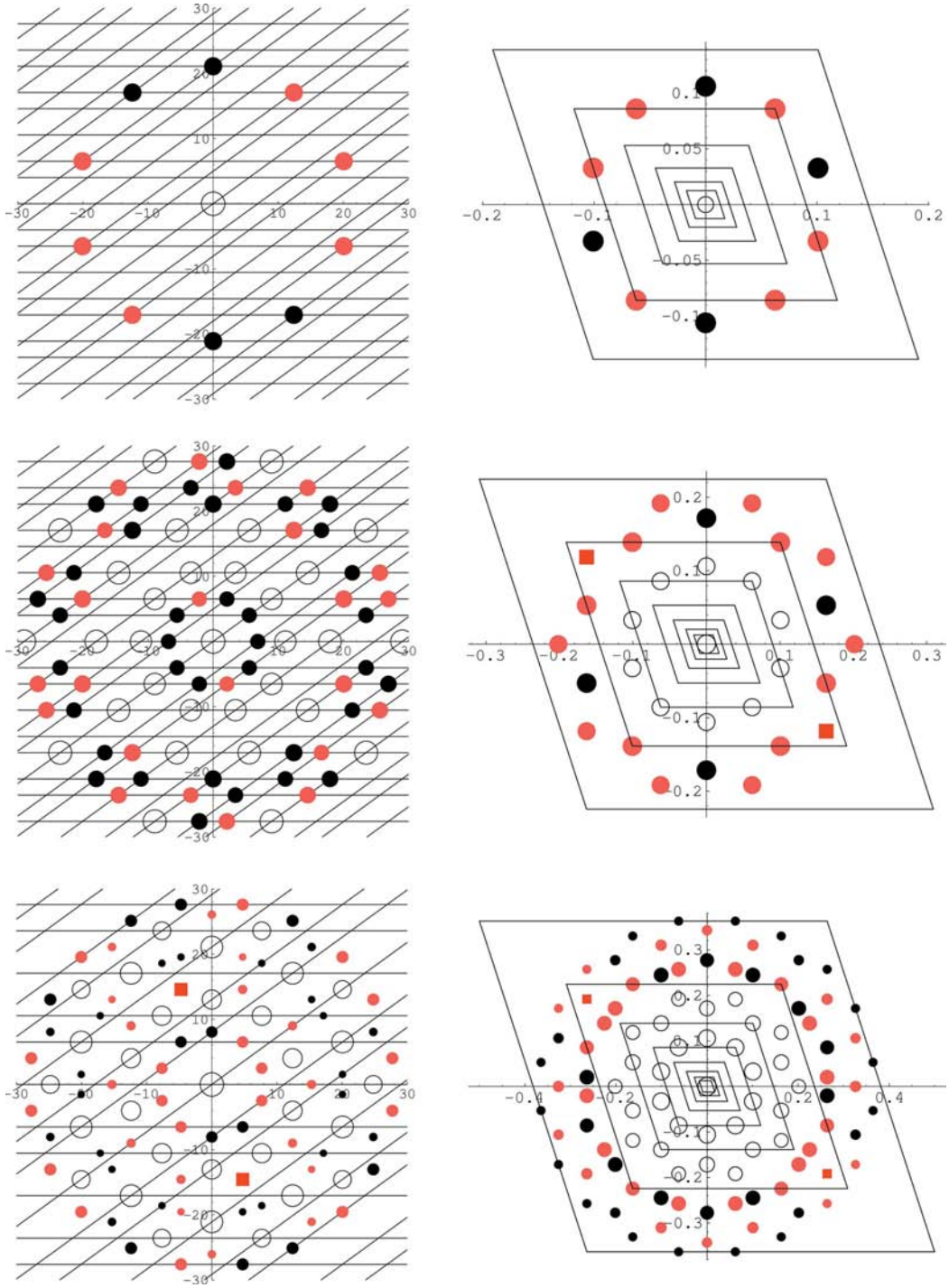

Figure 14
Penrose set diffraction-pattern partition: top $R_{5,4}$, $R_{5,5}$; middle $R_{6,4}$, $R_{6,5}$ and $R_{6,6}$; bottom $R_{7,5}$, $R_{7,6}$ and $R_{7,7}$.

Table 11
Partition of a random set with $\Phi_{max} = 0.2$.

	j								
X_i	0	1	2	3	4	5	6	7	8
$X_0 = 1$	1								
$X_2 = 0.985285$		2	8						
$X_3 = 0.961868$			2	8					
$X_4 = 0.902804$				2	8				
$X_5 = 0.76262$					24	36			
$X_6 = 0.479748$					2	34	44		
$X_7 = 0.115008$						10	136	146	
$X_8 = 0.02$							30	126	92

Table 12
Partition of a random set with $\Phi_{max} = 1$.

	j							
X_i	0	1	2	3	4	5	6	7
$X_0 = 1$	1							
$X_2 = 0.963035$		2	8					
$X_3 = 0.905867$			2	8				
$X_4 = 0.770592$				2	8			
$X_5 = 0.498559$					24	36		
$X_6 = 0.140072$					2	34	44	
$X_7 = 0.02$						10	78	50

8. Pertinence of the multiresolution partition

We have presented partitions of diffraction patterns based on the β-numeration, which naturally emerges as an efficient tool every time the number β is involved as an inflation factor, possibly combined with rotational symmetries, as is the case for quasicrystals. Note that the β-numeration has already been introduced in Elkharrat (2004*a*,*b*) to label the Bragg peaks of one-dimensional quasiperiodic structures. It has been used in the building of function bases, such as wavelet bases (Andrle *et al.*, 2004), and in the building of space symmetry groups for β-lattices (Elkharrat *et al.*, 2004). Finally, it is an efficient tool for characterizing Voronoi cells of β-lattices (Elkharrat & Frougny, 2005).

Let us now give some indication of the interest of the multiresolution partition of diffraction patterns of aperiodic sets.

We are experimenting with a new method. The essential part of the pure point information can be read at once, thanks to the $R_{i,j}$ array. The set of the $R_{i,j}$'s are, so to speak, the 'fingerprints' of the structure. If the diffraction pattern of the latter is purely observational, finitely different fingerprints are possible, depending on the orientation, as discussed in §6.2. Then the set of such fingerprints will be viewed as the fingerprint of the structure. What we can observe from the $R_{i,j}$ components with regard to the chosen window in real space for cut-and-project sets is that there is a neat difference between sets like the β-grid itself or subsets of the latter filtered through a quite elementary window (pentagonal, decagonal, Gaussian, random, ...) and more elaborate models

Table 13
Partition of the Steurer and Kuo model for $l = 0$.

	j									
X_i	0	1	2	3	4	5	6	7	8	9
$X_6 = 51.65$						6	4			
$X_7 = 10.59$				2	16	28	36	28		
$X_9 = 3.8$		2	10	8	6	32	80	110	66	16

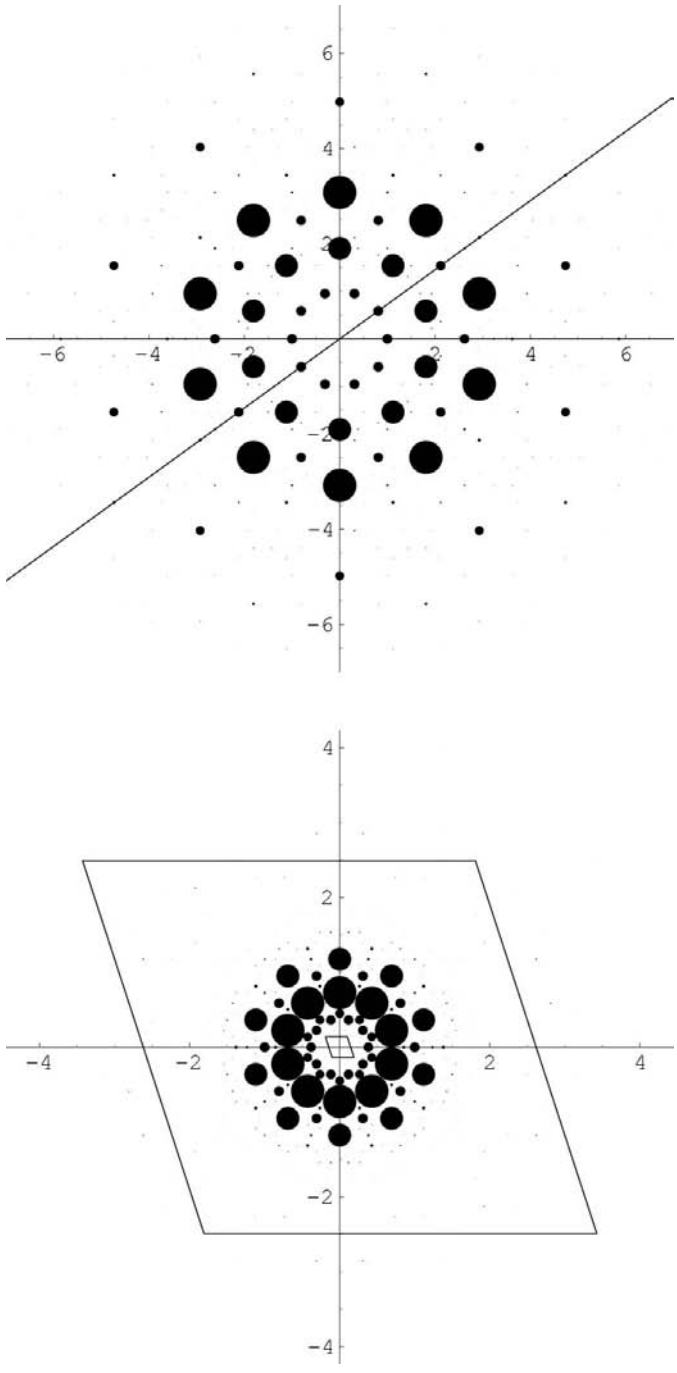

Figure 15
The diffraction pattern of the Steurer and Kuo model for the plane $l = 0$. Above: in the physical space together with the grid $\mathcal{G}_0$; below: in the internal space together with the envelope $\tau^8 R_\tau$.

Table 14
Partition of the Steurer and Kuo model for $l = 1$.

	j									
X_i	0	1	2	3	4	5	6	7	8	9
$X_5 = 30.19$			2	8	2	8				
$X_6 = 25.75$						4	16			
$X_7 = 9.72$					12	16	38	24		
$X_8 = 9.47$								4	16	
$X_9 = 5.56$						12	34	96	40	

Table 15
Partition of the Steurer and Kuo model for $l = 2$.

	j									
X_i	0	1	2	3	4	5	6	7	8	9
$X_6 = 38.38$						6	4			
$X_7 = 10.71$				2	16	28	36	28		
$X_8 = 6.98$					4	20	32	28	16	
$X_9 = 2.85$		2	8			4	54	142	122	28

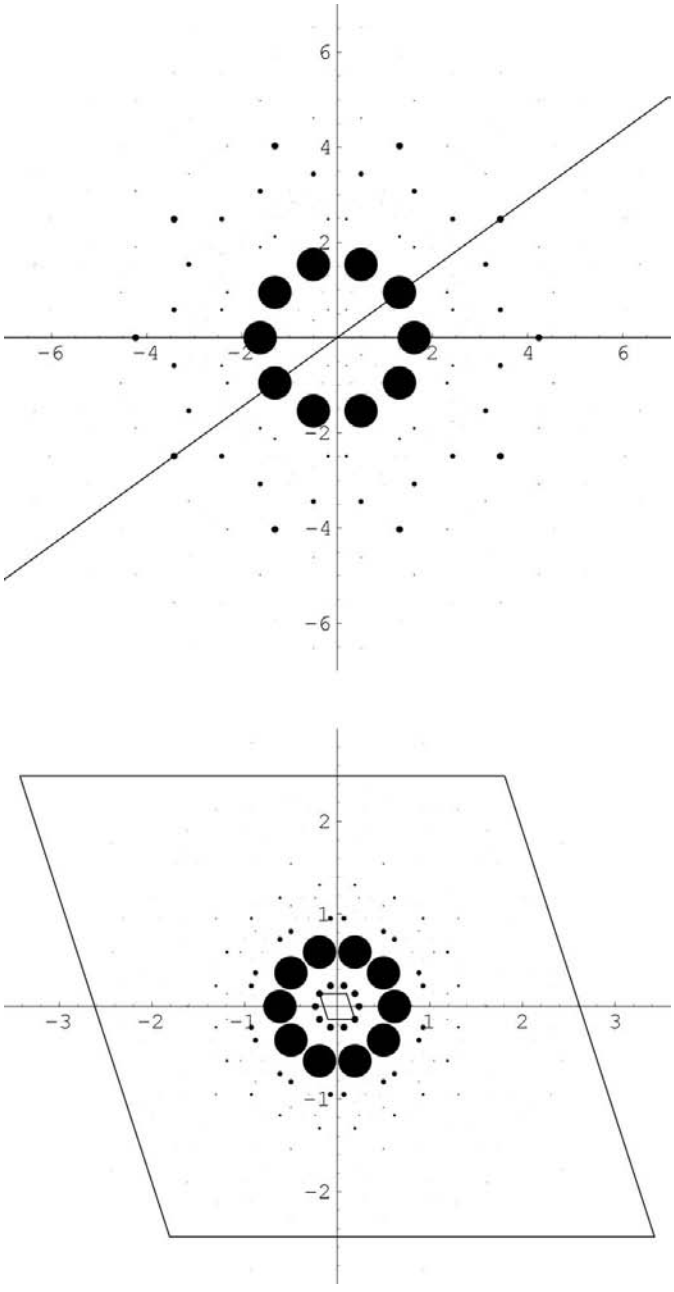

Figure 16
The diffraction pattern of the Steurer and Kuo model for the plane $l = 1$.

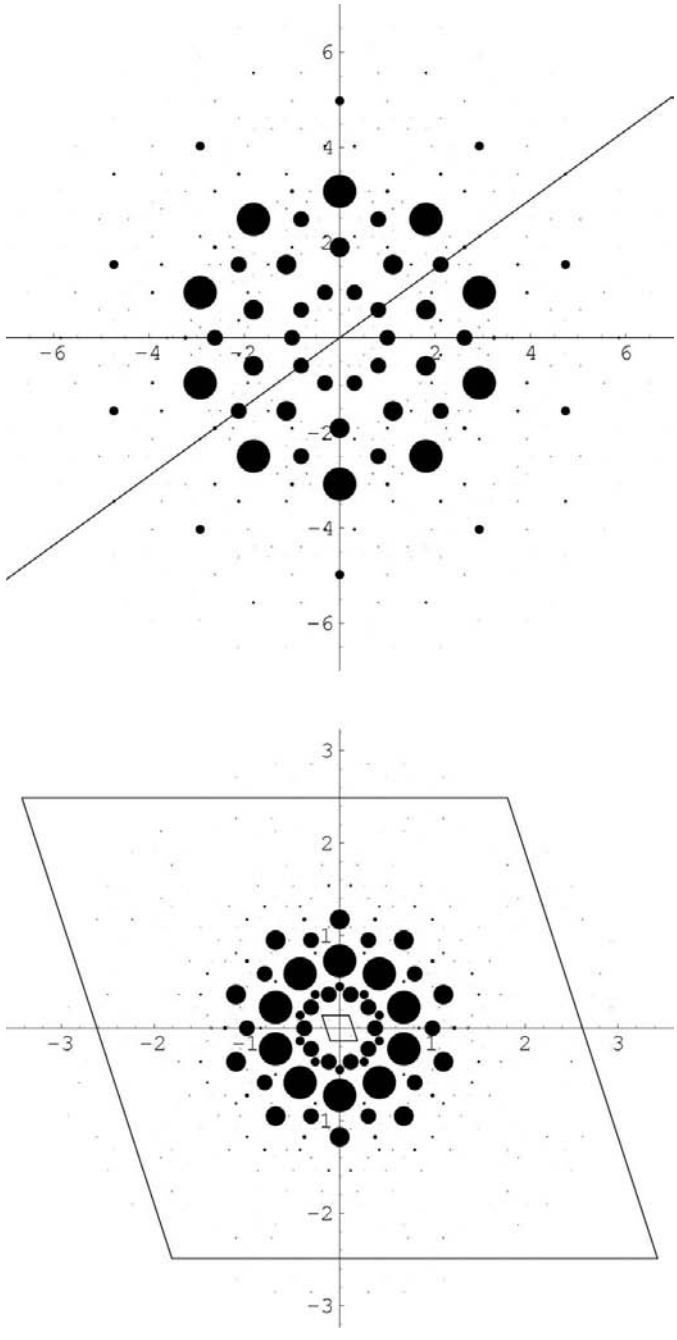

Figure 17
The diffraction pattern of the Steurer and Kuo model for the plane $l = 2$.

Table 16
Partition of the Steurer and Kuo model for $l = 3$.

	j									
X_i	0	1	2	3	4	5	6	7	8	9
$X_5 = 23.05$			2	8	2	8				
$X_6 = 19.19$						4	16			
$X_7 = 6.23$				2	20	16	52	40		
$X_8 = 6.11$								4	16	
$X_9 = 3.37$					4	28	24	92	72	

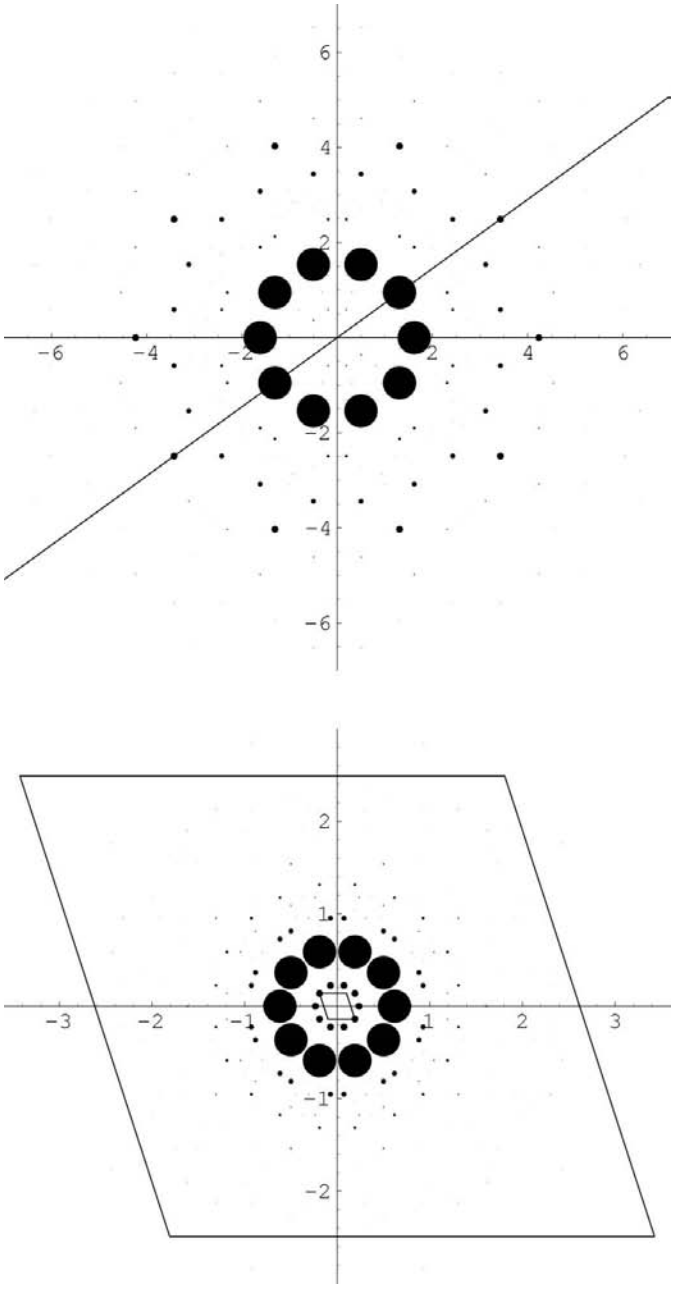

Figure 18
The diffraction pattern of the Steurer and Kuo model for the plane $l = 3$.

like Penrose sets or the Steurer–Kuo model, for which the filtering leads to more sparse occupation of τ-grid sites in real space and a combination of dense packing at lines X_7, X_8, X_9 and extinctions at earlier lines. This fact can be understood from the mathematics of diffraction of cut-and-project sets (in so far as the latter are QC realistic models): the more elaborate the construction of the window is in terms of multiplication by more-or-less localized functions (departing from characteristic functions), the more irregular is the distribution of the Bragg peaks in terms of intensity and scale (departing from simple convolution with sinc). Hence, one can loosely conclude that our 'fingerprints' easily discriminate between simplistic models and supposedly more realistic ones. Consequently, this partition eases the classification of aperiodic sets, as we have briefly seen with the numerical examples. On this basis, it would be interesting to extend this classification and to sort all the different structures, both theoretically and experimentally determined.

Of course, the partition does not give exhaustive information on the diffraction pattern. It is necessary to rely on complementary sources of information. For example, we obviously have no information on the continuous part of the pattern.

One can argue that the β-lattices are not symmetrical and thus destroy the natural symmetry of the problem. However, just a look at the figures displaying progressive multiresolutions of diffraction patterns clearly shows that the β-lattices do not destroy the symmetry. They are precisely built to comply with existing symmetry constraints as much as possible. Of course, they do not have themselves rotational symmetries like a cut-and-project set with a suitable symmetric window would have, but indubitably their 'neutrality' with regard to any kind of symmetry related to β is an advantage. Choosing instead a point set with given symmetry as a multiresolution background would introduce a bias in favor of that symmetry. It is in our opinion the deep meaning of 'β-lattices as universal labeling frame', built from the numeration system *naturally* adapted to the symmetry considered. As a matter of fact, in the case of $\beta = \tau = 2\cos(\pi/5)$, $\theta = \pi/5$ for the angle between the two axes appears likely to be the most 'economical' choice for including any union of cut-and-project sets with fivefold or tenfold symmetries [see, for instance, Burdík *et al.* (1998) or Gazeau & Krejcar (2000)].

One can also argue that the X_j and thus the cardinals of the sets P_j or $R_{i,j}$ might change as a function of a slight perturbation of the spectrum, as for all methods of classification based on a succession of cutoffs. These changes might be appreciable at large intensities (which are not crucially discriminating) but not at smaller intensities, where the cardinals become increasingly larger and, we believe, irrelevant with regard to a necessary comparative statistical analysis of the fingerprints.

A strong point of the partition, as compared to other methods, is a better readability of data derived from a diffraction pattern. Peaks are organized in a hierarchical fashion, according to their intensity level and according to

their scale level within the nested sequence of β-lattices. Moreover, each step of the multiresolution process unveils in a regular progressive way the rotational symmetries present in the original pattern (*e.g.* twofold, then tenfold for a ring of Bragg peaks). We are aware that the studies we have presented here have to be completed with comparative statistical analysis of the repartition of the $R_{i,j}$ *versus* academic examples as well as experimental data. This will be the aim of a future study.

As a final comment, it is likely that a large part of quasicrystallography can be expressed in terms of β-numeration. The multiresolution partition of diffraction patterns fostered by β-lattices is then a part of a whole system which allows quasicrystallography to be tackled in an altogether coherent way.

APPENDIX *A*
Algebraic objects: cyclotomic rings and PV numbers

Since we are concerned with the cyclotomic extension ring of the Nth root of unity $\zeta = \exp(i2\pi/N)$ defined by

$$\mathbb{Z}[\zeta] = \sum_{q=0}^{N-1} \mathbb{Z}\zeta^q = \mathbb{Z}[2\cos(2\pi/N)] + \mathbb{Z}[2\cos(2\pi/N)]\zeta,$$

we recall here some definitions on numbers together with the algebraic rings they generate.

The point set

$$\mathbb{Z}[\rho \equiv 2\cos(2\pi/N)]$$
$$\stackrel{\text{def}}{=} \{m_1 + m_2\rho + \ldots + m_{q_N}\rho^{q_N-1} \mid m_1, m_2, \ldots, m_{q_N} \in \mathbb{Z}\}$$

is the extension ring on the integers of the algebraic integer $2\cos(2\pi/N)$, with q_N the degree of its minimal polynomial.

In the noncrystallographic cases Pisot–Vijayaraghavan (PV) numbers are involved.

Definition 2. A Pisot–Vijayaraghavan, or PV, number $\beta > 1$ is an algebraic integer, dominant root of the polynomial

$$P(X) = X^n - a_{n-1}X^{n-1} - \ldots - a_1X - a_0,$$

with $a_0, \ldots, a_{n-1} \in \mathbb{Z}$, such that the modulus of each of its Galois conjugates, *i.e.* the other roots of $P(X)$, is strictly smaller than 1. It is said to be a unit if $a_0 = \pm 1$.

Denote by $\mathbb{Z}[\beta] = \{m_0 + m_1\beta + \ldots + m_{n-1}\beta^{n-1} \mid m_i \in \mathbb{Z}\}$ the extension ring generated by such a β.

Definition 3. A cyclotomic PV number with symmetry of order N is a PV number β such that

$$\mathbb{Z}[\beta] = \mathbb{Z}[2\cos(2\pi/N)].$$

Hence we have for such cyclotomic PV numbers[2]

$$\mathbb{Z}[\zeta] = \mathbb{Z}[\beta] + \mathbb{Z}[\beta]\zeta. \tag{29}$$

The set $\mathbb{Z}[\zeta]$ is clearly invariant under rotation of order N about the origin, because of the relation $\zeta^2 = \rho\zeta - 1 \in \mathbb{Z}[\zeta]$, and is a natural framework for two-dimensional structures having β as an inflation factor and $2\pi/N$ as a rotational symmetry, as arises in quasicrystallography.

Examples of such cyclotomic PV numbers are precisely those listed in cases 1 and 2.

APPENDIX *B*
The basics of β-numeration and β-integers

Everyone is familiar with the binary system used to express real numbers as series in powers of 2:

$$\mathbb{R} \ni x = \pm(x_j2^j + x_{j-1}2^{j-1} + \ldots + x_l2^l + \ldots), \tag{30}$$

where $j = j(x) \in \mathbb{Z}$ is the highest power of 2 such that $2^j \leq |x| < 2^{j+1}$, x_j = integral part of $|x|/2^j \equiv [|x|/2^j] \in \{0, 1\}$. The other expansion coefficients $x_l \in \{0, 1\}$ are inductively defined by $x_l = [2r_{l+1}]$, r_l = fractional part of $2r_{l+1} \equiv \{2r_{l+1}\}$, with $r_j = \{|x|/2^j\}$. As a consequence, a positive x is a word, $x_jx_{j-1}\ldots x_1x_0 \cdot x_{-1}x_{-2}\ldots$, made with letters x_l in the alphabet $\{0, 1\}$. The standard ordering of the positive real numbers corresponds to the lexicographical ordering of those words, and the natural numbers are those for which $x_l = 0$ for all $l < 0$. The same algorithm, called a greedy algorithm, can be employed to represent real numbers in a system based on an *arbitrary* real number $\beta > 1$: $\mathbb{R} \ni x = \pm(x_j\beta^j + x_{j-1}\beta^{j-1} + \ldots + x_l\beta^l + \ldots) \equiv \pm x_jx_{j-1}\ldots x_1x_0 \cdot x_{-1}x_{-2}\ldots$, where the 'letters' assume their values in the alphabet $\{0, 1, \ldots, \beta - 1\}$ if β is natural, and $\lfloor\beta\rfloor$ if β is not. But if β is not natural, not all words are allowed.

Let us see how this works in the case $\beta = \tau$. Since $\tau = 1.618\ldots$, the alphabet is $\{0, 1\}$, and so any positive x is represented in 'basis τ' by

$$x = \sum_{l=-\infty}^{j} x_l\tau^l \equiv x_jx_{j-1}\ldots x_1x_0 \cdot x_{-1}x_{-2}\ldots, \tag{31}$$

where $x_l \in \{0, 1\}$, *and* $x_{l+1}x_l = 0$. The latter 'forbidding rule' expresses the algebraic fact that $\tau^{l+1} + \tau^l = \tau^{l+2}$. So, any 1 in the τ-expansion (31) has to be followed by 0 whereas 0 can be followed by 0 or 1. All allowed words can be lexicographically ordered following that constraint and this order corresponds to the standard order on the real line. By definition, the positive τ-integers are those real numbers which have only positive powers of τ in their τ-expansion (31). So, we will denote them by

$$\mathbb{Z}_\tau^+ = \left\{x = \sum_{l=0}^{j} x_l\tau^l,\ x_l \in \{0, 1\},\ x_lx_{l+1} = 0\right\}. \tag{32}$$

Accordingly, the set of τ-integers is defined by

$$\mathbb{Z}_\tau = \mathbb{Z}_\tau^+ \cup (-\mathbb{Z}_\tau^+).$$

For instance, the first positive τ-integers are given by

[2] See Bell & Hare (2005), where a complete classification of Pisot cyclotomic numbers for degrees 2, 3 and 4 is given, along with some examples of higher degree.

$$\overbrace{0}^{1}\ \overbrace{1}^{1/\tau}\ \overbrace{\tau}^{1}\ \tau^2$$
$$(0)\quad (0)\quad (10)\quad (100)$$

$$\overbrace{\ }^{1}\ \overbrace{\tau^2+1}^{1/\tau}\ \overbrace{\tau^3}^{1}\ \tau^3+1$$
$$(101)\quad (1000)\quad (1001).$$

We thus obtain a sequence of numbers strictly increasing in steps of length equal to 1 or $1/\tau$. In a certain sense, this quasiperiodic sequence with two incommensurable periods is closest to the periodic one with period equal to 1, namely the sequence of the integers.

Generalization of this example is straightforward.

Definition 4. The set of β-integers is the set of real numbers such that their β-expansions have a β-fractional part equal to 0,

$$\begin{aligned}\mathbb{Z}_\beta &= \{x \in \mathbb{R} \mid \langle |x| \rangle = x_k x_{k-1} \ldots x_1 x_0\} \\ &= \mathbb{Z}_\beta^+ \cup \mathbb{Z}_\beta^-,\end{aligned} \tag{33}$$

where $\mathbb{Z}_\beta^+$ is the set of non-negative β-integers and $\mathbb{Z}_\beta^- = -\mathbb{Z}_\beta^+$.

For the other β of interest in quasicrystallography, the first positive β-integers read as

$$\mathbb{Z}_\delta^+ = \{0, 1, 2, \delta, \delta+1, \delta+2, 2\delta, \delta^2, \delta^2+1, \ldots\},$$
$$\mathbb{Z}_\gamma^+ = \{0, 1, 2, \gamma, \gamma+1, \gamma+2, 2\gamma, 2\gamma+1, \gamma^2, \gamma^2+1, \ldots\},$$
$$\mathbb{Z}_\theta^+ = \{0, 1, 2, 3, \theta, \theta+1, \theta+2, \theta+3, 2\theta, 2\theta+1, 2\theta+2, \ldots\}.$$

APPENDIX C
Scaled β-integers and nested decompositions of extension rings

Here we prove that the set $\mathbb{Z}[\beta]$, for β a quadratic Pisot unit, is the inductive limit of nested sequences of (possibly decorated) scaled versions of $\mathbb{Z}_\beta$.

Let us first explain how the construction of the set of β-integers is related to the algebraic cut-and-project algorithm (Berman & Moody, 1994). The Galois conjugation is the map

$$x = m + n\beta \mapsto x' = m + n\beta', \tag{34}$$

where $m, n \in \mathbb{Z}$. Now define the aperiodic set Σ^Ω,

$$\Sigma^\Omega = \{x \in \mathbb{Z}[\beta] \mid x' \in \Omega\},$$

where Ω, referred to as the window of Σ^Ω, is a bounded subset of $\mathbb{R}$ with non-empty interior, see Moody & Patera (1994) and Moody (1997). The sets of non-negative and non-positive β-integers are given by the following equations (Frougny *et al.*, 2003; Burdík *et al.*, 1998).

Case 1:

$$\begin{aligned}\mathbb{Z}_\beta^+ &= \Sigma^{(-1,\beta)} \cap \mathbb{R}^+, \\ \mathbb{Z}_\beta^- &= \Sigma^{(-\beta,1)} \cap \mathbb{R}^-.\end{aligned} \tag{35}$$

Case 2:

$$\begin{aligned}\mathbb{Z}_\beta^+ &= \Sigma^{[0,\beta)} \cap \mathbb{R}^+, \\ \mathbb{Z}_\beta^- &= \Sigma^{(-\beta,0]} \cap \mathbb{R}^-.\end{aligned} \tag{36}$$

We are now interested in the decomposition of the set $\mathbb{Z}[\beta]$, *i.e.* the support of diffraction patterns produced by one-dimensional aperiodic sets, using the nested sequence of subsets $(\mathbb{Z}_\beta/\beta^j)_{j\in\mathbb{Z}}$. Recall that the sets of β-integers are self-similar sets obeying

$$\ldots \subset \mathbb{Z}_\beta/\beta^{j-1} \subset \mathbb{Z}_\beta/\beta^j \subset \mathbb{Z}_\beta/\beta^{j+1} \subset \ldots \subset \mathbb{Z}[\beta] \tag{37}$$

with $j \in \mathbb{Z}$. Note that equation (37) does not necessarily mean that $\mathbb{Z}[\beta]$ is the limit of the sequence $(\mathbb{Z}_\beta/\beta^j)_{j\in\mathbb{Z}}$, in the sense of Definition 1, as we shall see in the following.

Case 1.

In the algebraic cut-and-project formalism, the sequence $(\mathbb{Z}_\beta/\beta^j)_{j\in\mathbb{Z}}$ reads

$$\begin{aligned}\mathbb{Z}_\beta^+/\beta^j &= \Sigma^{(-\beta^j,\beta^{j+1})} \cap \mathbb{R}^+, \\ \mathbb{Z}_\beta^-/\beta^j &= \Sigma^{(-\beta^{j+1},\beta^j)} \cap \mathbb{R}^-,\end{aligned}$$

with $j \in \mathbb{Z}$. These equations show that $\mathbb{Z}[\beta]$ is the limit of the sequence $(\mathbb{Z}_\beta/\beta^j)$,

$$\lim_{j\to\infty} \left(\mathbb{Z}_\beta/\beta^j\right) = \mathbb{Z}[\beta]. \tag{38}$$

Thus, we have a partition of $\mathbb{Z}[\beta]$, in terms of the self-similar, inflated or deflated versions of $\mathbb{Z}_\beta$.

Case 2.

In the algebraic cut-and-project formalism, the sequence $(\mathbb{Z}_\beta/\beta^j)_{j\in\mathbb{Z}}$ reads

$$\begin{aligned}\mathbb{Z}_\beta^+/\beta^j &= \Sigma^{[0,\beta^{j+1})} \cap \mathbb{R}^+, \\ \mathbb{Z}_\beta^-/\beta^j &= \Sigma^{(-\beta^{j+1},0]} \cap \mathbb{R}^-,\end{aligned}$$

with $j \in \mathbb{Z}$. In this case, it is clear that we cannot find an approximation sequence for $\mathbb{Z}[\beta]$ like in equation (38). Nevertheless, we can recover such a nested approximation sequence if we use the decorated set of β-integers

$$\widetilde{\mathbb{Z}}_\beta = \mathbb{Z}_\beta + \{0, \pm 1/\beta\},$$

which reads, in the cut-and-project formalism,

$$\widetilde{\mathbb{Z}}_\beta^+ = \Sigma^{(-\beta,2\beta)} \cap \mathbb{R}^+, \quad \widetilde{\mathbb{Z}}_\beta^+/\beta^j = \Sigma^{(-\beta^{j+1},2\beta^{j+1})} \cap \mathbb{R}^+,$$
$$\widetilde{\mathbb{Z}}_\beta^- = \Sigma^{(-2\beta,\beta)} \cap \mathbb{R}^-, \quad \widetilde{\mathbb{Z}}_\beta^-/\beta^j = \Sigma^{(-2\beta^{j+1},\beta^{j+1})} \cap \mathbb{R}^-,$$

with $j \in \mathbb{Z}$. We now have

$$\lim_{j\to\infty} \left(\widetilde{\mathbb{Z}}_\beta/\beta^j\right) = \mathbb{Z}[\beta]. \tag{39}$$

When the number β is a quadratic PV unit, as is the case here, such a decomposition is immediate. However, when the degree of the minimal polynomial is greater than 2, this

question is highly non-trivial (Akiyama *et al.*, 2004; Sidorov, 2003). A complete study of the approximation of $\mathbb{Z}[\tau]$ by the nested sequence $(\mathbb{Z}_\tau/\tau^j)_{j\in\mathbb{Z}}$ can be found in Elkharrat (2004*a*,*b*), together with the partition of diffraction measures it generates, and with some numerical examples.

APPENDIX *D*
Penrose point set within the cut-and-project framework

The algebraic construction of the set of nodes of a standard or singular Penrose tiling is not immediate. Here we first recall the main steps of such a construction based on algebraic filtering and coloring in $\mathbb{Z}[\zeta = \exp[i(2\pi/5)]]$, following Moody & Patera (1994). We next explain how the same construction can be achieved by sieving τ-lattices (Gazeau & Krejcar, 2000).

Denote by $\phi : \mathbb{Z}[\zeta] \mapsto \mathbb{Z}_5 \equiv \mathbb{Z}/5\mathbb{Z}$ the coloring ring homomorphism given by

$$\begin{aligned} z &= n_4\zeta^4 + n_3\zeta^3 + n_2\zeta^2 + n_1\zeta + n_0 \\ &\mapsto \phi(z) = n_4 - n_3 + n_2 - n_1 + n_0 \bmod 5. \end{aligned}$$

The fact that the integer on the right-hand side of the equation is defined modulo 5 is trivially due to the relation $\zeta^4 - \zeta^3 + \zeta^2 - \zeta + 1 = 0$. The color of a $z \in \mathbb{Z}[\zeta]$ is left unchanged under star mapping, and we have $\phi(\zeta^*) = (\phi(\zeta))^3 = -1$. Let Ω_1 denote the pentagonal convex hull of the set $\{1, \zeta^2, \zeta^4, \zeta^6, \zeta^8\}$, $\Omega_2 = -\tau\Omega_1$, $\Omega_3 = \tau\Omega_1$ and $\Omega_4 = -\Omega_1$, the vertices of which are of colors 1, 2, 3 and 4, respectively. Let then the set $\Sigma^{\Omega_k} \subset \mathbb{Z}[\zeta]$ be defined by

$$\Sigma^{\Omega_k} = \{z \in \mathbb{Z}[\zeta] \mid z^* \in \Omega_k,\ \phi(z) = k\}.$$

One example of a (singular) Penrose set $\mathcal{P}$ is the union of the four 'colored' sets Σ^{Ω_k},

$$\mathcal{P} = \bigcup_{k=1}^{4} \Sigma^{\Omega_k}. \tag{40}$$

Note that this point set is fivefold rotationally invariant about the origin. It is obvious from equation (10) that the Penrose set defined in equation (40) is not embedded in $\Gamma(\tau)$, but its inflated version is,

$$\begin{aligned} \tau\mathcal{P} &= \bigcup_{k=1}^{4} \tau\Sigma_k^{\Omega} \\ &= \left\{z \in \Gamma(\tau) \mid z^* \in -(1/\tau)\Omega_k,\ \phi(z) = 3k \bmod 5\right\}. \end{aligned}$$

We thank both referees for their very constructive remarks. They pointed out many problems in our original text and their comments, criticisms and questions helped us great deal to correct and improve our work.

References

Akiyama, S., Rao, H. & Steiner, W. (2004). *J. Number Theory*, **107** 135–160.

Andrle, M., Burdík, Č. & Gazeau, J. P. (2004). *J. Fourier Anal. Appl.* **10**, 269–300.

Baake, M. & Moody, R. V. (2000). Editors. *Directions in Mathematical Quasicrystals*, CRM Monograph Series. Providence: American Mathematical Society.

Barache, D., Champagne, B. & Gazeau, J. P. (1998). Fields Institute Monograph Series, No. 10, pp. 15–66. Providence: American Mathematical Society.

Bell, J. P. & Hare, K. G. (2005). *J. Number Theory*, **115**, 215–229.

Berman, S. & Moody, R. V. (1994). *J. Phys. A Math. Gen.* **27**, 115–129.

Bruijn, N. G. de (1981*a*). *Indagationes Math.* **84**, 39–52.

Bruijn, N. G. de (1981*b*). *Indagationes Math.* **84**, 53–66.

Burdík, Č., Frougny, Ch., Gazeau, J. P. & Krejcar, R. (1998). *J. Phys. A Math. Gen.* **31**, 6449–6472.

Elkharrat, A. (2004*a*). *Eur. Phys. J.* **B39**, 287–294.

Elkharrat, A. (2004*b*). Thesis, Université Paris 7 – Denis Diderot, France.

Elkharrat, A. & Frougny, Ch. (2005). In *Developments in Language Theory: 9th International Conference, DLT 2005, Palermo, Italy, July 4–8, 2005*, edited by C. De Felice & A. Restivo, *Lecture Notes in Computer Science*, Vol. 3572, pp. 209–215. Berlin, Heidelberg: Springer.

Elkharrat, A., Frougny, Ch., Gazeau, J. P. & Verger-Gaugry, J. L. (2004). *Theor. Comput. Sci.* **319/1–3**, 281–305.

Fettweis, M. (1994). PhD thesis, Université Paris XI – Orsay, France.

Fettweis, M., Launois, P., Reich, R., Wittmann, R. & Dénoyer, F. (1995). *Phys. Rev. B*, **51**, 6700–6703.

Frougny, Ch., Gazeau, J. P. & Krejcar, R. (2003). *Theor. Comput. Sci.* **303**, 491–516.

Gazeau, J. P. & Krejcar, R. (2000). *From Quasicrystals to More Complex Systems*, edited by F. Axel, F. Denoyer & J.-P. Gazeau. Berlin, New York: Springer/Cambridge, Les Ulis: EDP Sciences.

Gazeau, J. P. & Verger-Gaugry, J.-L. (2006). *Ann. Inst. Fourier*, **56**, 2441–2465.

Hof, A. (1995). *Commun. Math. Phys.* **169**, 25–43.

Janot, C. (1996). *Quasicrystals, A Primer*. Oxford University Press.

Levine, D. & Steinhardt, P. J. (1986). *Phys. Rev. B*, **34**, 596–616.

Mallat, S. (1989). *Trans. Am. Math. Soc.* **315**, 69–87.

Meyer, Y. (1995). *Beyond Quasicrystals*, edited by F. Axel & D. Gratias. Berlin: Les éditions de physique/Springer-Verlag.

Moody, R. (1997). In *The Mathematics of Long-Range Aperiodic Order*, edited by R. Moody. Dordrecht: Kluwer.

Moody, R. V. & Patera, J. (1994). *Can. J. Phys.* **72**, 442–452.

Schlottmann, M. (1998). *Quasicrystals and Discrete Geometry*, edited by J. Patera, pp. 247–264. Fields Institute Monograph Series, No. 10. Providence: American Mathematical Society.

Schlottmann, M. (2000). *Directions in Mathematical Quasicrystals*, edited by M. Baake & R. V. Moody. CRM Monograph Series. Providence: American Mathematical Society.

Shechtman, D., Blech, I., Gratias, D. & Cahn, J. W. (1984). *Phys. Rev. Lett.* **53**, 1951–1953.

Sidorov, N. (2003). *Period. Math. Hung.* **47**, 221–231.

Steurer, W. & Kuo, K. H. (1990*a*). *Acta Cryst.* B**46**, 703–712.

Steurer, W. & Kuo, K. H. (1990*b*). *Philos. Mag. Lett.* **62**, 175–182.